Monte Carlo studies of quantum phase transitions

Kunal Verma (MS18148)

Master's Dissertation

Department of Physical Sciences
Indian Institute of Science Education and Research
(IISER) Mohali

First Draft: 10th April 2023

Supervisor: Prof. Sanjeev Kumar   Co-supervisor: Prof. Vijay B. Shenoy

Certificate of Examination

This is to certify that the dissertation titled **Monte Carlo studies of quantum phase transitions** submitted by **Kunal Verma** (Reg. No. MS18148) for the partial fulfillment of BS- MS Dual Degree programme of the institute, has been examined by the thesis committee duly appointed by the institute. The committee finds the work done by the candidate satisfactory and recommends that the report be accepted.

Prof. Sanjeev Kumar   Dr. Abhishek Chaudhari   Dr. Yogesh Singh

Prof. Sanjeev Kumar
(Supervisor)

Dated: 10th April 2023

Declaration

The work presented in this dissertation has been carried out by me under the guidance of Prof. Sanjeev Kumar at the Indian Institute of Science Education and Research, Mohali.

This work has not been submitted in part or in full for a degree, a diploma, or a fellowship to any other university or institute. Whenever contributions of others are involved, every effort is made to indicate this clearly, with due acknowledgement of collaborative research and discussions. This thesis is a bonafide record of original work done by me and all sources listed within have been detailed in the bibliography.

Kunal Verma
(Candidate)
Dated: 10th April 2023

In my capacity as the supervisor of the candidates project work, I certify that the above statements by the candidate are true to the best of my knowledge.

Prof. Sanjeev Kumar
(Supervisor)
Dated: 10th April 2023

Acknowledgements

Use this section to acknowledge the help/contribution of others.

Abstract

Use this section to include an abstract of the thesis.

List of Figures

Contents

1 Monte Carlo simulations

The purpose of this chapter is to give a brief introduction to Monte Carlo simulations and their applications in the numerical analysis of phase transitions in statistical physics models. We will start by illustrating the general idea of importance sampling Monte Carlo methods, followed by the different type of update schemes (Metropolis, Wolff-cluster, etc.) to sample non-uniform distributions efficiently. We will also pay attention to the topic of statistical analysis of the generated data via autocorrelation analysis and statistical error analysis. For illustration purposes, we will primarily focus our attention on the simplest spin model, i.e., the two-dimensional Ising model (without external field) and discuss the finite-temperature critical phenomena and phase transition. Finally, we will demonstrate the calculation of the critical exponents of the two-dimensional Ising model using finite-size scaling analysis of relevant physical observables. Although we start with a classical statistical model, these ideas can be generalized and are applicable in simulations of quantum-spin systems, where they become the *Quantum Monte Carlo* (QMC) methods [Janke, Sandvik].

1.1 Introduction to Monte Carlo

Monte Carlo simulations are an important and broad class of stochastic methods that utilize randomness to solve deterministic problems efficiently. To show their utility, we will start with a simple and illustrative example. Consider the calculation of a thermal expectation value of an observable $Q(x)$ in statistical physics;

$$\langle Q \rangle = \int_0^L \mathrm{d}x\, \rho(x)Q(x), \qquad \int_0^L \mathrm{d}x\, \rho(x) = 1, \qquad (1.1.1)$$

where $\rho(x)$ is the underlying probability distribution.

The most naive way to estimate this integral numerically is to use *Euler's method* to

discretize the integration range into N pieces and perform a discretized sum

$$\langle Q \rangle \approx \Delta x \sum_{j=1}^{N} \rho(x_0 + j\Delta x)\, Q(x_0 + j\Delta x) \qquad (1.1.2)$$

where $\Delta x = L/N$. Such grid-based methods are very accurate for low-dimensional integrals, but as we go to higher-dimensional integrals, both the error-scaling and computational costs grow significantly.

A more efficient method for performing high-dimensional integrals is known as *Monte Carlo integration* where the points are uniformly sampled across the integration range instead of a grid. If the uniformly sampled random points are denoted by the set $\{x_1, x_2, x_3, \ldots, x_N\}$, then the integral in Eq. (1.1.1) can be estimated as

$$\langle Q \rangle \approx \frac{L}{N} \sum_{i=1}^{N} \rho(x_i)\, Q(x_i) \qquad (1.1.3)$$

The error in a Monte Carlo estimate goes as $1/\sqrt{N}$ in any number of dimensions, and hence it is more efficient for estimating $6\mathcal{N}$-dimensional integrals characteristic of statistical mechanics of $\mathcal{N}$ particles. However, this straightforward unbiased Monte Carlo integration only works well in practice if the integrand isn't sharply peaked in some small region of the integration range.
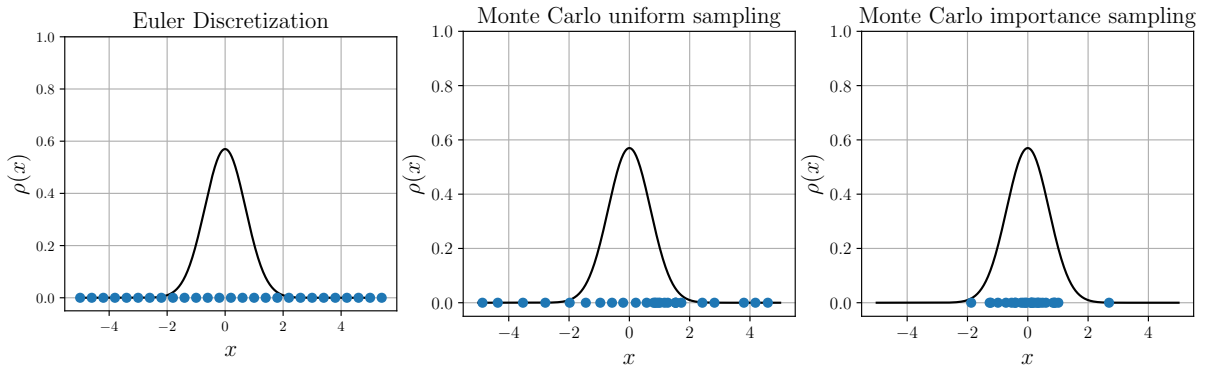
Figure 1.1: Comparision of sampling techniques.

If $\rho(x)$ is sharply peaked in a small region, then uniform sampling of points can result in large statistical fluctuations as only a small fraction of points will fall within the dominant range. Therefore, the next improvement can be performed by sampling the points according to a probability distribution $W(x)$ which is peaked in the same region as $\rho(x)$. This gives the estimate of the expectation value as

$$\langle Q \rangle \approx \frac{L}{N} \sum_{i=1}^{N} \frac{\rho(x_i)}{W(x_i)} Q(x_i)\, W(x_i) \approx \frac{1}{N} \sum_{i=1}^{N}{}^{(W)} \frac{\rho(x_i)}{W(x_i)}\, Q(x_i) \qquad (1.1.4)$$

where $\sum^{(W)}$ denotes points being sampled from the distribution $W(x)$, and we write

$L \sum W(x_i) \to \sum^{(W)}$. Often, a good solution is to use $W(x) = \rho(x)$, and the expectation value becomes an arithmetic average of $Q(x)$ over the configurations sampled by $\rho(x)$

$$\langle Q \rangle \approx \frac{1}{N} \sum_{i=1}^{N}{}^{(\rho)} Q(x_i) \tag{1.1.5}$$

This technique is known as the *Monte Carlo Importance Sampling* method since we are only sampling the points lying in the "important" region of the probability distribution $\rho(x)$.

In statistical mechanics, the probability distribution is generally the Boltzmann distribution $\rho(\vec{x}, \vec{p}) = e^{-\beta H(\vec{x}, \vec{p})}$, and we can use Monte Carlo importance sampling to calculate expectation values of physical observables. However, in the above discussion, we have ignored the problem of sampling points according to a given probability distribution. We discuss this in the following subsection.

1.1.1 Detailed Balance condition

In order to calculate integrals via the method of importance sampling, we need a way to sample points according to the probability distribution $\rho(x)$. The theory of Markov Chains provides us with the necessary tools to generate a Markov Chain process which evolves towards a desired equilibrium distribution.

In physicists' language, a Markov chain is a discrete chain of events $C_1 \to C_2 \to C_3 \to \ldots \to C_N$ that evolves stochastically and satisfies the Markovian property, i.e., the probability of $C_{i-1} \to C_i$ transition is independent of its history. Put together, this implies the probability of obtaining the above sequence is

$$P(C_1 \to C_2 \to \ldots \to C_N) = P(C_1) \cdot P(C_2|C_1) \cdot P(C_3|C_2) \ldots P(C_N|C_{N-1}) \tag{1.1.6}$$

Roughly speaking, if the Markov chain doesn't repeat itself and can reach *any* configuration starting from *any other* configuration, then it is *ergodic* and settles onto a stationary distribution. By designing an appropriate Markov chain, it is possible to obtain any desired stationary distribution $\rho(C)$.

Let us now assume we have a set of all possible configurations $\{X\} = \{X_1, X_2, \ldots, X_n\}$ in the configuration space. Assume we start with some configuration $X_{i(0)}$ and stochastically generate a Markov chain $X_{i(1)}, X_{i(2)}, X_{i(3)}, \ldots, X_{i(M)}$. We can do the same for an ensemble of configurations initially distributed according to $\rho(X)$. At the update 0 , the number of configurations X_i in the initial ensemble is $N_0(X_i) \propto \rho(X_i) \Rightarrow N_0(X_i) = \mathcal{N}\rho(X_i)$. The given Markov chain must have an update scheme which stochastically evolves the ensemble to the next set of states. The number of configurations after the update 1 is

$$N_1(X_i) = N_0(X_i) + \sum_{j \neq i} [N_0(X_j) \, P(X_j \to X_i) - N_0(C_i) \, P(X_i \to X_j)] \tag{1.1.7}$$

The first term in the sum represents configurations updating into X_i and the second term represents X_i updating out to other configurations. If we want the ensemble to remain distributed according to the initial ensemble distribution $\rho(X)$, then, for all $i = 1, 2, \ldots M$,

$$\sum_{j \neq i} \left[\rho(X_j) \, P(X_j \to X_i) - \rho(C_i) \, P(X_i \to X_j) \right] \overset{!}{=} 0 \qquad (1.1.8)$$

One possible solution of this condition is to satisfy it term-by-term $\forall \ j$

$$\rho(X_j) \, P(X_j \to X_i) - \rho(C_i) \, P(X_i \to X_j) \overset{!}{=} 0 \qquad (1.1.9)$$

which can be written as a ratio

$$\frac{P(X_j \to X_i)}{P(X_i \to X_j)} = \frac{\rho(X_i)}{\rho(X_j)}, \qquad (1.1.10)$$

also known as the *detailed balance condition*. Although here we start with an ensemble distributed according to the probability distribution ρ, for practical purposes, neither do we need to start from the same distribution, nor do we require an ensemble of configurations. In practice, the master equation Eq. (1.1.7) takes care of the excess or deficiency and equilibrates after a characteristic *equilibration time* of Markov chain updates.

The transition probability $P(X_i \to X_j)$ can further be written as a product of the update proposal and the proposal acceptance probabilities

$$P(X_i \to X_j) = \underbrace{\mathcal{A}(X_i \to X_j)}_{\text{propose } X_i \to X_j} \cdot \underbrace{P_{\text{accept}}(X_i \to X_j)}_{\text{accept } X_i \to X_j} \qquad (1.1.11)$$

Since the proposal probabilities should be uniform $\mathcal{A}(X_i \to X_j) = \text{constant}$, the detailed balance condition in terms of acceptance probabilities becomes

$$\frac{P_{\text{accept}}(X_j \to X_i)}{P_{\text{accept}}(X_i \to X_j)} = \frac{\rho(X_i)}{\rho(X_j)} \qquad (1.1.12)$$

Starting from the detailed balance condition, one can define stochastic algorithms, such as Monte Carlo simulations, which generate configurations according to a desired distribution. One such common algorithm is the *Metropolis algorithm* with the solution to Eq. (1.1.12) as

$$P_{\text{accept}}(X_i \to X_j) = \min \left[\frac{\rho(X_j)}{\rho(X_i)}, 1 \right] \qquad (1.1.13)$$

For statistical mechanics, the desired equilibrium distribution is the Boltzmann distribution which gives rise to the well-known Metropolis acceptance probability

$$P_{\text{accept}}(E_i \to E_j) = \min \left[e^{-\beta(E_j - E_i)}, 1 \right]. \qquad (1.1.14)$$

1.2 Metropolis and the Ising model

As discussed in the last section, we can generate samples distributed according to the Boltzmann distribution if we choose the acceptance probability as defined in Eq. (1.1.14) for the Markov chain. These drawn configurations can then be utilized to calculate thermal expectation values via importance sampling.

We will discuss this simulation method in the context of the 2-dimensional ferromagnetic Ising model. The Ising model is the paradigmatic model for systems exhibiting continuous phase transition from a ferromagnetic to a paramagnetic phase at a critical temperature T_c. In the absence of an external field ($h = 0$) and only nearest-neighbor interactions, the energy of the ferromagnetic Ising model is

$$E = -J \sum_{\langle i,j \rangle} \sigma_i \sigma_j \tag{1.2.1}$$

where $\langle i, j \rangle$ indicates nearest-neighbors i, j and the expression for a 2-dimensional square lattice can be more suggestively written as

$$E = -J \sum_i \sigma_{i_x,i_y} \left[\sigma_{i_x,i_y+1} + \sigma_{i_x+1,i_y} \right] \tag{1.2.2}$$

For a Markov chain transition $\sigma_i \to -\sigma_i$, the difference in energy between the configurations is given by

$$\Delta E = 2J \, \sigma_{i_x,i_y} \left[\sigma_{i_x,i_y+1} + \sigma_{i_x+1,i_y} + \sigma_{i_x,i_y-1} + \sigma_{i_x-1,i_y} \right] \tag{1.2.3}$$

This leads to the Metropolis acceptance probability for the Ising model spin flips being given by

$$P_{\text{accept}}(\sigma_i \to -\sigma_i) = \min \left[e^{-\beta \Delta E}, 1 \right] \tag{1.2.4}$$

with ΔE being defined by Eq. (1.2.3). In a nutshell, a *Metropolis Monte Carlo* simulation of the Ising model consists of performing such spin flip proposals by selecting the spin σ_i to be flipped at random and generating a Markov chain distributed according to the Boltzmann distribution. A single *Monte Carlo sweep* then consists of L^2 such spin flip proposals so that roughly each lattice site gets an equal chance to flip, where L denotes the side length of the square lattice. As a step-by-step procedure, a Monte Carlo sweep is defined as follows:

1. Randomly choose a spin σ_i on the lattice.

2. Propose the spin flip $\sigma_i \to -\sigma_i$.

3. Calculate the difference in energy $\Delta E = E_{\text{final}} - E_{\text{initial}}$.

4. Accept the proposed move with a probability of $\min \left[e^{-\beta \Delta E}, 1 \right]$.

5. Steps 1 to 4 are then repeated $\mathcal{N} = L^2$ times.

The Boltzmann sampling performed using Markov Chain Monte Carlo (MCMC) can then be utilized in calculating expectation values of observables as simple statistical averages over the sampled points

$$\langle \mathcal{O} \rangle \approx \frac{1}{N} \sum_{\{\sigma\}} \mathcal{O}(\sigma) \tag{1.2.5}$$

where we have suppressed the superscript $^{(\rho)}$ on the sum denoting sampling over the distribution $\rho(\{\sigma\}) = e^{-\beta E(\{\sigma\})}$. Note that such Monte Carlo averages are always supposed to be taken over *equilibrated* configurations in a Monte Carlo simulation. As discussed earlier, the master equation (1.1.7) ensures the equilibration of the Markov chain's probability distribution after a few steps by taking care of appropriate excess or deficiencies during the initial steps. This initial equilibration period where no measurements are performed is known as the *equilibration time* or the *thermalization time*, often denoted by t_{eq}.

The Metropolis MCMC method is thus a conceptually simple and quite universally applicable algorithm. Its applications range from simulations of simple Ising chains to highly non-trivial spin systems. However, the Metropolis algorithm comes with its fair share of problems which we will discuss later. In the next section, we will discuss the relevant statistical physics of the Ising model and the measurement of physical observables.

1.3   Physical quantities

To set the scenery for calculating observable expectation values, we will first begin by discussing the relevant physical observables for the Ising model. Since we are dealing with spin systems, a natural quantity of interest is the magnetization, which acts as the *order parameter* of the Ising phase transition at $T_c \neq 0$. The magnetization per site is defined by the observable

$$m \equiv \frac{1}{\mathcal{N}} \sum_{i=1}^{\mathcal{N}} \sigma_i \tag{1.3.1}$$

where $\mathcal{N} = L^2$ is the total number of lattice sites. One can explicitly check that an operation which rotates all spins $\sigma_i \to -\sigma_i \; \forall \, i$ is a symmetry of the Ising Hamiltonian (Eq. (1.2.1)). Although we are technically not yet dealing with quantum mechanics, this operation can be denoted as $F = \prod_{i=1}^{N} X_i$ where X_i denotes a flip of spin at site i. Since applying this operation twice is equivalent to identity ($F^2 = \mathbb{1}$), we often say that the Ising model possesses a global $\mathbb{Z}_2$ symmetry.

As a result of this global $\mathbb{Z}_2$ symmetry, both negative and positive magnetization are equally probable. However, in the thermodynamic limit $\mathcal{N} \to \infty$ (infinitely large lattice), if the system attains a state with spins predominantly in one direction below $T < T_c$, then it cannot spontaneously (in a finite time) fluctuate through a series of local spin flips into a state with the opposite magnetization. This is known as the *spontaneous symmetry-breaking* of the global $\mathbb{Z}_2$ symmetry in the Ising model, and can be physically thought of as arising from the limit of a very weak external field. However, in a finite system, such

fluctuations are possible and it is possible for $\langle m \rangle = 0$ for all temperatures T, making it difficult to study the phase transition which appears in the thermodynamic limit.

Therefore, in simulations of finite lattice sizes, **we instead define the order parameter as $\langle |\boldsymbol{m}| \rangle$.** As the system size increases, the $\langle |m| \rangle$ curve sharpens close to T_c and approaches the thermodynamic limit symmetry-broken $\langle m(T) \rangle$ curve.

Similarly, the other relevant physical observable is the energy density which is simply defined as the energy per site

$$e = \frac{E}{\mathcal{N}} = \frac{-J}{\mathcal{N}} \sum_{\langle i,j \rangle} \sigma_i \sigma_j \tag{1.3.2}$$

We can also use magnetization and energy density observables to calculate other derived quantities of interest. In the context of magnetization, we can calculate the magnetic susceptibility

$$\chi \equiv \left. \frac{\partial \langle M \rangle}{\partial h} \right|_{h=0} \tag{1.3.3}$$

i.e. the linear response of magnetization in the weak field limit, i.e., $E' = \lim_{h \to 0}(E - hM)$. It is easy to show that the expression for susceptibility simplifies to

$$\chi = \frac{1}{T}\left(\langle M^2 \rangle - \langle |M| \rangle^2\right) = \frac{L^2}{T}\left(\langle m^2 \rangle - \langle |m| \rangle^2\right) \tag{1.3.4}$$

where we have replaced the $\langle m \rangle$ with $\langle |m| \rangle$ for reasons discussed previously. Similarly, the specific heat capacity is another quantity of interest which is defined as

$$C_V = \frac{\partial \langle E \rangle}{\partial T} = \frac{L^2}{T^2}\left(\langle e^2 \rangle - \langle e \rangle^2\right) \tag{1.3.5}$$

Finally, we are also interested in the derived *Binder cumulant* which is defined as the kurtosis of the order parameter $\langle |m| \rangle$

$$U_L = 1 - \frac{\langle m^2 \rangle_L}{3 \langle m^2 \rangle_L}, \tag{1.3.6}$$

and the intersection of U_L curves for different lattice side L is used to accurately determine the phase transition point.

Therefore, the measurements of the set of physical observables $\{|m|, m^2, m^4, e, e^2\}$ is sufficient to determine the Q vs. T curves for all the relevant observables $(e, |m|)$ and derived quantities (χ, C_V, U_L). Using Monte Carlo simulations, we can calculate the expectation values and statistical errors in these quantities, and use the simulation data to extract the critical exponents, which we will discuss in later sections.

1.4 Autocorrelation functions

All MCMC algorithms are based upon the central idea of performing local or cluster updates to arrive at the next configuration (or the next state in a Markov chain). Naturally, it is reasonable to expect that the observable measurements are temporally correlated and these correlations are quite significant near the transition points. The only way to get around this is to perform the measurements of the observables after a few time steps so as to ensure that subsequent measurements are statistically uncorrelated. The *autocorrelation function* is a quantitative measure of temporal correlations between measurements. For an observable $\mathcal{O}$, the autocorrelation function is defined as

$$A_{\mathcal{O}}(t) = \frac{1}{N-t} \sum_{k=0}^{N-t-1} \frac{(\mathcal{O}(k) - \langle \mathcal{O} \rangle) \cdot (\mathcal{O}(k+t) - \langle \mathcal{O} \rangle)}{\langle \mathcal{O}^2 \rangle - \langle \mathcal{O} \rangle^2} \tag{1.4.1}$$

where $\mathcal{O}(k)$'s are the measurements performed at each MC sweep, and N is the total number of MC sampling sweeps. Moreover, the averages in Eq. (1.4.1) are calculated only over the first $N-t$ measurements.

$$\langle \mathcal{O}^n \rangle = \frac{1}{N-t} \sum_{k=0}^{N-t-1} [\mathcal{O}(k)]^n \tag{1.4.2}$$

The autocorrelation function is suitably normalized to give values $\in [-1,1]$. For an ergodic simulation, we expect $A_{\mathcal{O}}(t) \to 0$ as $t \to \infty$; infact, $A_{\mathcal{O}}(t)$ is expected to fall off as an exponential

$$A_{\mathcal{O}}(t) \sim e^{-|t|/\tau}, \tag{1.4.3}$$

and τ is called the *autocorrelation time*. The autocorrelation time is roughly the number of MC steps after which the temporal correlations drop to $1/e \approx 0.37$. A general rule of thumb in MCMC simulations is to **perform measurements of the observables after every 2τ steps.** For an observable $\mathcal{O}$, we define the *integrated autocorrelation time* τ_{int} as a discretized integration sum

$$\tau_{\text{int},\mathcal{O}} = \frac{1}{2} \sum_{t=-\infty}^{\infty} A_{\mathcal{O}}(t) = \frac{1}{2} + \sum_{t=1}^{\infty} A_{\mathcal{O}}(t) \tag{1.4.4}$$

However, this natural estimator isn't *quite* correct because the autocorrelations $A_{\mathcal{O}}(t)$ for $t \gg \tau_{\text{int}}$ contain much noise and little signal. To fix this, we implement the *automatic windowing algorithm* [Sokal] by introducing a cutoff M on the sum

$$\tau_{\text{int},\mathcal{O}} = \frac{1}{2} + \sum_{t=1}^{M} A_{\mathcal{O}}(t) \tag{1.4.5}$$

M is chosen as the smallest integer such that $M \geq 6\tau_{\text{int},\mathcal{O}}(M)$. The algorithm can be summarized as follows

1. Start with some small value of M, say $M = 50$, and evaluate $\tau_{\text{int},\mathcal{O}}(50)$.

2. Check if $50 \geq 6\tau_{\text{int},\mathcal{O}}(50)$.

3. If not, increase the value of M and repeat until you find a M where $M \geq 6\tau_{\text{int},\mathcal{O}}(M)$.

We take the autocorrelation time τ_{int} of a given (L, T) simulation as the maximum of autocorrelation times for all observables except magnetization m. This is because the lack of symmetry-breaking in finite lattices causes the time taken to tunnel between positive and negative m states to be very long, leading to extremely high autocorrelations.

$$\tau_{\text{int}} = \max \left\{ \tau_{\text{int},|m|}, \ \tau_{\text{int},m^2}, \ \tau_{\text{int},m^4}, \ \tau_{\text{int},e}, \ \tau_{\text{int},e^2} \right\} \tag{1.4.6}$$

The first run of the simulation is only used to calculate the integrated autocorrelation time τ_{int}, followed by a second run where measurements are taken after every $2\tau_{\text{int}}$ steps. These statistically independent measurements can then be used to compute the Monte Carlo expectation values and errors.
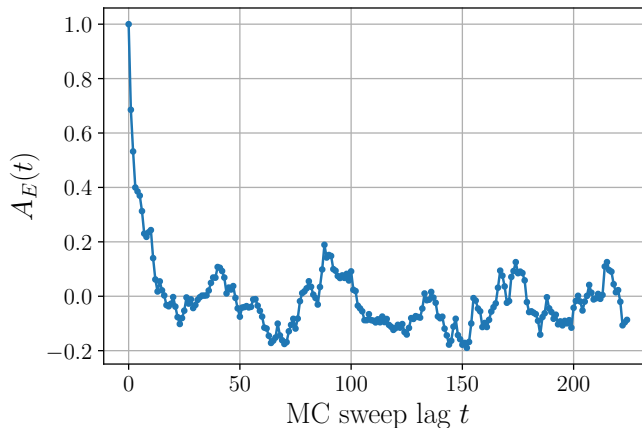
Figure 1.2: Exponential decay of energy density autocorrelation function.

1.5 Expectation values and errors

Once we have a set of uncorrelated Monte Carlo observable measurements, it is a simple task to calculate the mean and standard deviation of the uncorrelated observable measurement data $(|m|, e)$. However, for quantities that are not measured directly in the simulation but are computed as non-linear combinations of basic observables (χ, C_V, U_L), deriving a propagated error is a highly non-trivial task. Therefore, we utilize *Jackknife analysis* to create large blocks/bins of the data and perform the required computations.

1.5.1 Jackknife binning analysis

We begin by binning the N measurements of observable $\mathcal{O}$ into N_B non-overlapping bins of length k such that $N_B k = N$, and construct a shorter time series of bin averages. The

bin average for the jth bin is defined as

$$\mathcal{O}_j^{(B)} \equiv \frac{1}{k} \sum_{i=0}^{k-1} \mathcal{O}_{jk+i} \tag{1.5.1}$$

Below is a visual representation of the binning process

$$\{\underbrace{\{\mathcal{O}_0, \mathcal{O}_1 \dots \mathcal{O}_{k-1}\}}_{\overline{\mathcal{O}}_0^{(B)}}, \underbrace{\{\mathcal{O}_k, \mathcal{O}_{k+1} \dots \mathcal{O}_{2k-1}\}}_{\overline{\mathcal{O}}_1^{(B)}}, \dots \dots, \underbrace{\{\mathcal{O}_{(N_B-1)k}, \mathcal{O}_{(N_B-1)k+1} \dots \mathcal{O}_{N-1}\}}_{\overline{\mathcal{O}}_{N_B-1}^{(B)}}\}$$

$$\Downarrow$$

$$\{\overline{\mathcal{O}}_0^{(B)}, \overline{\mathcal{O}}_1^{(B)}, \overline{\mathcal{O}}_2^{(B)} \dots, \overline{\mathcal{O}}_{N_B-1}^{(B)}\}$$

Knowing the bin averages for the observables $\mathcal{O} \in \{|m|, m^2, m^4, e, e^2\}$, the bin estimates of the derived quantities are estimated as

$$\chi_j^{(B)} = \beta \, L^2 \left(\overline{m^2}_j^{(B)} - \left[\overline{|m|}_j^{(B)} \right]^2 \right) \tag{1.5.2}$$

$$C_{V}{}_j^{(B)} = \beta^2 \, L^2 \left(\overline{e^2}_j^{(B)} - \left[\overline{e}_j^{(B)} \right]^2 \right) \tag{1.5.3}$$

$$U_L{}_j^{(B)} = 1 - \frac{\overline{m^4}_j^{(B)}}{3 \left[\overline{m^2}_j^{(B)} \right]^2} \tag{1.5.4}$$

We denote these derived quantities by ρ such that $\rho \in \{\chi, C_V, U_L\}$. The means over the bin averages (for $\mathcal{O}$) and bin estimates (for ρ) are also calculated

$$\overline{\mathcal{O}} = \overline{\overline{\mathcal{O}}_j^{(B)}} = \frac{1}{N_B} \sum_{i=0}^{N_B-1} \overline{\mathcal{O}}_j^{(B)} \tag{1.5.5a}$$

$$\overline{\rho} = \overline{\rho_j^{(B)}} = \frac{1}{N_B} \sum_{i=0}^{N_B-1} \rho_j^{(B)} \tag{1.5.5b}$$

For the Jackknife error analysis, we begin by constructing the same number (N_B) of Jackknife bins containing all data but the jth bin of the previously mentioned binning method. The Jackknife averages for these new bins are defined as

$$\overline{\mathcal{O}}_j^{(J)} = \frac{N\overline{\mathcal{O}} - k\overline{\mathcal{O}}_j^{(B)}}{N - k} \tag{1.5.6}$$

$$\overline{\rho}_j^{(J)} = \frac{N\overline{\rho} - k\rho_j^{(B)}}{N - k} \tag{1.5.7}$$

Since we are using the same data again and again while forming the Jackknife bins, these bins are trivially correlated, and as a result, the Jackknife bin variance is much smaller than is expected. This can be corrected by multiplying the sample variance by another

factor of $(N_B - 1)^2$ resulting in

$$\delta\overline{\mathcal{O}} = \sqrt{\frac{N_B - 1}{N_B} \sum_{j=0}^{N_B-1} \left(\overline{\mathcal{O}}_j^{(J)} - \overline{\mathcal{O}}\right)^2} \qquad (1.5.8a)$$

$$\delta\rho = \sqrt{\frac{N_B - 1}{N_B} \sum_{j=0}^{N_B-1} \left(\overline{\rho}_j^{(J)} - \overline{\rho}\right)^2} \qquad (1.5.8b)$$

Therefore, using the calculated values from Eq. (1.5.5) and Eq. (1.5.8), we get our mean and error estimates of the observable expectation values and the derived physical quantities

$$\text{Estimate of } \langle\mathcal{O}\rangle \to \overline{\mathcal{O}} \pm \delta\overline{\mathcal{O}}, \qquad \text{Estimate of } \rho \to \overline{\rho} \pm \delta\rho$$

1.6 Critical slowing down

Phase transitions, in general, are associated with a discontinuity in the first derivative (for first-order phase transitions) or a divergence in the second derivative (for second-order phase transitions). For example, the classical Ising model is characterized by a second-order phase transition at a critical temperature T_c. Above this temperature ($T > T_c$), the spins are randomly aligned and correspond to the *paramagnetic* phase. Below this temperature ($T < T_c$), the spins majorly align in one of the directions to form the *ferromagnetic* phase of the system. In the paramagnetic phase, at high temperatures, the

(a) Domain formation near T_c ($T = 2.30$).

(b) High autocorrelation times near T_c for Metropolis.
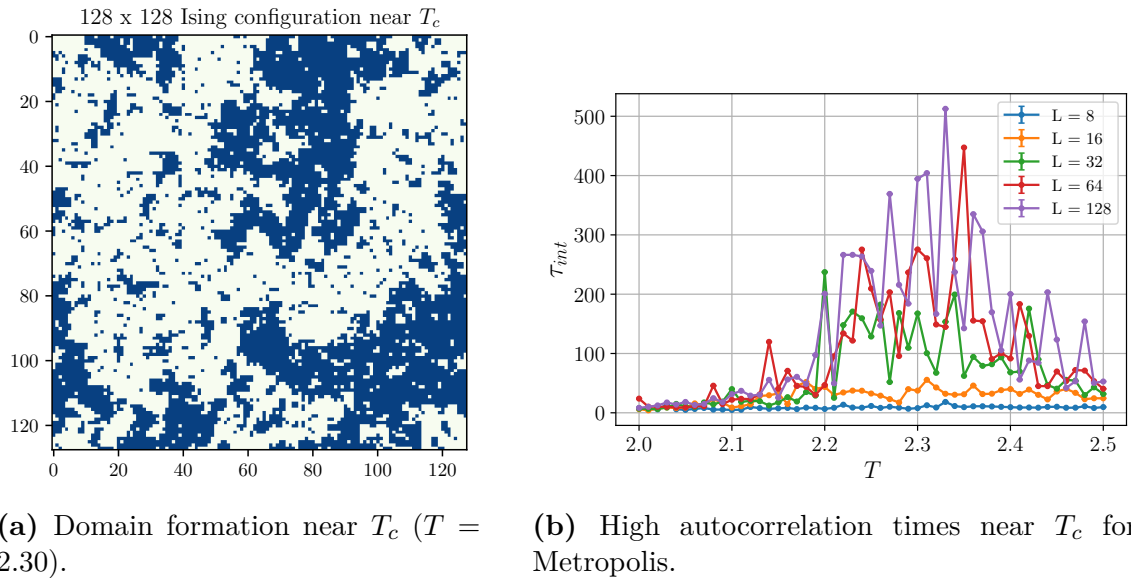
Figure 1.3: Critical slowing down near the transition point in the Ising model.

spin configuration is random and there are little to no spatial correlations. However, as the temperature decreases, we enter the paramagnetic phase and spins tend to align themselves with their neighbors. As a result, we form large *domains* or *clusters* of spins

and we have a high degree of spatial correlation (Fig. 1.3a), often measured by the parameter ξ, known as the correlation length. As one approaches the critical temperature T_c from the above, the onset of strong correlations results in *domain flips* which cause high fluctuations in magnetization and energy. Since the Metropolis algorithm performs local updates and the spins have a strong spatial correlation, we need to wait for a long autocorrelation time to get independent subsequent measurements (Fig. 1.3b). This is known in literature as *critical slowing down.*

The phenomena of critical slowing down is primarily dependent on the algorithm used. Since local update (such as Metropolis) take a long time to flip the domains and generate statistically independent configurations, they have a significantly higher computational cost as a tradeoff to their conceptual simplicity.

Therefore, it should be intuitively clear that some sort of non-local updates should be able to alleviate this problem by flipping entire clusters of spins. This class of algorithms is generally known as *Cluster-update algorithms.* Although the critical slowing down can be significantly reduced with cluster algorithms, they are still far less general applicable than local update algorithms.

1.7 Wolff Cluster algorithm

The acceptance probability of local update algorithms is very low around the critical regions making it an inefficient way to probe the critical properties of the system. In this section, we will discuss the *Wolff cluster algorithm*, which is a generalization of the Swendsen-Wang clyster dynamics and is even more efficient. The Wolff cluster algorithm works by identifying domains of identically oriented spins and performing a flip operation on the entire cluster [Krauth].

1.7.1 Deriving the probabilities

We will start by considering the example of two states a and b which differ by flipping of a cluster of identically oriented spins.

This can be done by starting the construction of a cluster which starts by seeding a random spin and iteratively adding neighboring sites of the same spin with a probability p. This means if a spin i is in the cluster, and a neighboring site j is not (and if $\sigma_i = \sigma_j$), then the link $\langle i, j \rangle$ should be added into the cluster with a probability p. Once the construction has stopped, we will still have n_{same} identical spin links just outside the cluster boundary which were not added into the cluster. Similarly, we say the number of opposite spin links which have a spin opposite to that of the cluster is n_{opp}. Also, $n_{\text{same}} + n_{\text{opp}} = N$ where N is the total number of links the cluster makes with outside spins.

Since the probability of a site not being accepted into the cluster is $(1 - p)$, the "a-priori" probability of proposing a cluster flip from $a \to b$ is

$$\mathcal{A}(a \to b) = \mathcal{A}_{\text{interior}} \cdot (1 - p)^{n_{\text{same}}}, \tag{1.7.1}$$

where $\mathcal{A}_{\text{interior}}$ is just a product of probabilities for links that were accepted into the cluster. In the reverse direction, if we would have started with the state b and tried constructing a cluster and flipping it to go to state a, the "a-priori" probability to propose a cluster flip from $b \to a$ is

$$\mathcal{A}(b \to a) = \mathcal{A}_{\text{interior}} \cdot (1-p)^{n_{\text{opp}}} \tag{1.7.2}$$

because in state b, the unaccepted but identical spins were exactly those which had the opposite spin in state a. Therefore, if we invoke the detailed balance condition Eq. (1.1.10) for the cluster flips to get

$$\frac{\mathcal{A}(a \to b) \cdot P_{\text{accept}}(a \to b)}{\mathcal{A}(b \to a) \cdot P_{\text{accept}}(b \to a)} = e^{-\beta(E_b - E_a)} \tag{1.7.3}$$

Now the energies of states a and b can be computed as nearest neighbor interaction *inside the cluster* and the interaction *outside the cluster*. Since a and b only differ by a cluster flip, the only difference appears in the interaction at the cluster boundary

$$E_a = E_{\text{interior}} + E_{\text{exterior}} - n_{\text{same}}J + n_{\text{opp}}J, \tag{1.7.4a}$$

$$E_b = E_{\text{interior}} + E_{\text{exterior}} - n_{\text{opp}}J + n_{\text{same}}J \tag{1.7.4b}$$

$$\implies E_b - E_a = 2J(n_{\text{same}} - n_{\text{opp}}) \tag{1.7.4c}$$

Therefore, putting in the expressions into the detailed balance condition, we get

$$\frac{P_{\text{accept}}(b \to a)}{P_{\text{accept}}(a \to b)} = e^{-2\beta J(n_{\text{same}} - n_{\text{opp}})}(1-p)^{n_{\text{opp}} - n_{\text{same}}} \tag{1.7.5a}$$

$$\implies \frac{P_{\text{accept}}(b \to a)}{P_{\text{accept}}(a \to b)} = \left(\frac{e^{-2\beta J}}{1-p}\right)^{n_{\text{same}} - n_{\text{opp}}} \tag{1.7.5b}$$

Thus, given a value of p (which can be a function of β and J), we can get the corresponding acceptance probability for the cluster algorithm. An interesting coincidence occurs when

$$p = 1 - \exp(-2\beta J). \tag{1.7.6}$$

This special choice of probability function yields a *rejection-free* algorithm whose acceptance probability is always 1.

$$\left.\frac{P_{\text{accept}}(b \to a)}{P_{\text{accept}}(a \to b)}\right|_{p=1-\exp(-2\beta J)} = \left(\frac{e^{-2\beta J}}{e^{-2\beta J}}\right)^{n_{\text{same}} - n_{\text{opp}}} = 1 \tag{1.7.7}$$

Thus, any proposed cluster construction and flipping is an always accepted move in the cluster algorithm. The cluster algorithm with the particular choice of $p = 1 - e^{-2\beta J}$ is known as the Wolff cluster algorithm.

1.7.2 Implementation

In this subsection, we will try to discuss an algorithmic implementation of Wolff clusters so that it can be easily coded into a Monte Carlo program.

Before starting, we will assume we are working with a 2-dimensional spin configuration and we aim to generate configurations distributed according to the Boltzmann distribution using Monte Carlo evolution with transition probabilities given by the Wolff scheme, which is the fastest currently known simulation method for the Ising model. One Wolff algorithm step is then defined in the following step-by-step procedure,

1. Randomly choose a site i on the lattice with the spin σ_i.

2. Label the neighbors of i as j. Add them to a temporary set. Call this set N_{temp}.

3. If $\sigma_i = \sigma_j$, add the neighbor j from set N_{temp} to the cluster $\mathcal{C}$ with a probability of $p = 1 - e^{-2\beta J}$.

4. Repeat step 2 for all the neighbors in set N_{temp}.

5. For sites that are *newly added* to the cluster, check for neighboring identical spins and add them to the cluster $\mathcal{C}$ by repeating steps 2 to 4.

6. Keep repeating till no more spins are added to the cluster $\mathcal{C}$.

7. Once the cluster is constructed, flip all the spins, i.e., $\forall\, j\, \in \mathcal{C}\,|\, \sigma_j \to -\sigma_j$.

More concisely, a single sweep of the Monte Carlo Wolff algorithm in `psuedocode language` is given below from [Krauth]. The sets $\mathcal{F}_{\text{old}}$ and $\mathcal{F}_{\text{new}}$ denote the frontier of the cluster at $(n-1)^{\text{th}}$ and n^{th} steps, respectively. The set $\mathcal{C}$ contains the sites belonging to the cluster.

algorithm wolff-cluster
begin
    $i :=$ random site;
    $\mathcal{C} := \{i\}$;
    $\mathcal{F}_{\text{old}} := \{i\}$;
    while $\mathcal{F}_{\text{old}} \neq \{\}$ **do**
    begin
        $\mathcal{F}_{\text{new}} := \{\}$;
        for $\forall\, i\, \in\, \mathcal{F}_{\text{old}}$ **do**
        begin
            for $\forall\, j$ neighbor of i with $\sigma_i = \sigma_j$, $j \notin \mathcal{C}$ **do**
            begin
                if $\text{ran}[0,1] < p$ **then**
                begin
                    $\mathcal{F}_{\text{new}} := \mathcal{F}_{\text{new}} \cup \{j\}$;
                    $\mathcal{C} := \mathcal{C} \cup \{j\}$;
                end

end
     end
     $\mathcal{F}_{\mathrm{old}} := \mathcal{F}_{\mathrm{new}}$;
  end
  for $\forall \; i \; \in \; \mathcal{C}$ **do**
  $\sigma_i := -\sigma_i$; **end**

The resulting dynamics is ergodic and obeys detailed balance.

1.8 Results

We have now setup our complete machinery for calculating physical observable expectation values (and errors) using Monte Carlo Wolff algorithm simulations. The workflow of the Monte Carlo code is summarized in the following section.

1.8.1 Structure of the code

The `ising` executable program calculates the expectation values of various observables and physical quantities derived from them, along with error bars. Each iteration of the program runs for a single (L, T) pair. The program is structured into four parts

    Part 1   A preliminary Monte Carlo run to collect autocorrelated observable measurements after the system equilibrates.

    Part 2   Calculation of the integrated autocorrelation time τ_{int} using the autocorrelated measurements.

    Part 3   The main Monte Carlo run with observable measurements being taken after every $2\tau_{\mathrm{int}}$ MC sweeps to ensure collection of uncorrelated measurements.

    Part 4   Calculating observable expectation values and derived physical quantities with error bars using jackknife binning method.

After obtaining the results of expectation values and derived physical quantities (with error bars) for a range of temperatures, we perform finite-size scaling analysis on the data to extract the critical exponents of the 2D Ising Model. The `ising-2d` source code is written in `C++` and the files can be accessed on the following link - ising-2d on GitHub.

1.8.2 Simulation results

The following parameters were used in the 2D Ising model simulations for lattice sizes of $L = 8, 16, 32, 64, 128$. Here, we have used the Wolff scheme to simulate the Markov chain Monte Carlo procedure instead of the Metropolis algorithm for reasons discussed in earlier sections. As a short remark on units, we are using the natural units where $k_B = 1$, so our units of temperature and energy are identical. We have also set the coupling paramater as unity `J = 1.0`.

For preliminary Monte Carlo (Part 1)

```
no of equilibration sweeps = 1.0e3

no of sampling sweeps = 1.0e4

sampling step size = 1.0e0
```
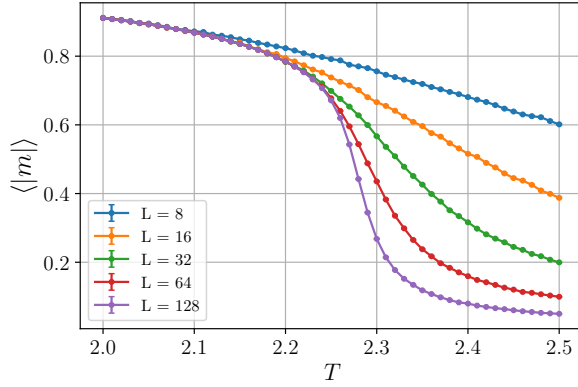
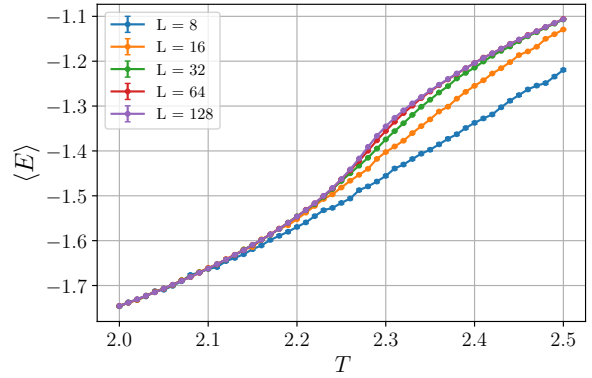**For the main Monte Carlo run (Part 3)**

```
no of equilibration sweeps = 1.0e3

no of sampling sweeps = 2τ · 2.0e4

sampling step size = 2τ
```
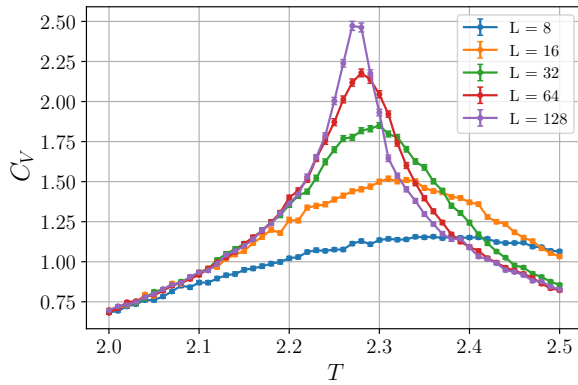

(a) $\langle |m| \rangle$ vs T

(b) $\langle e \rangle$ vs T

(c) C_V vs T

(d) χ vs T

(e) U_L vs T
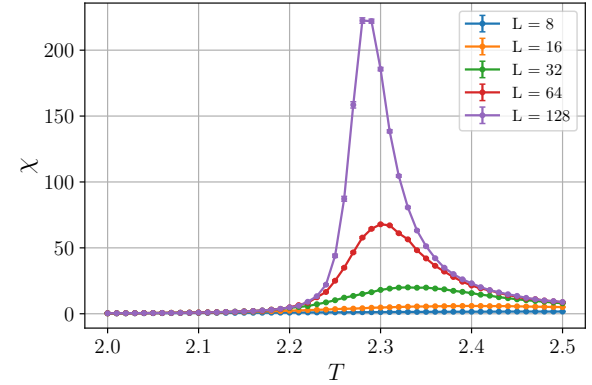
(f) τ_{int} vs T
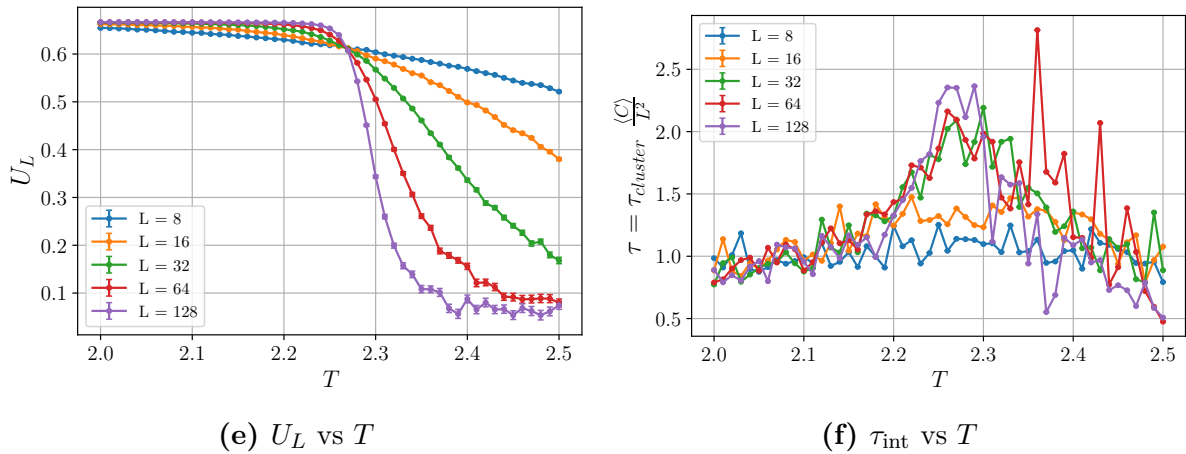
Figure 1.4: Variation of physical quantities with T for different lattice sizes L.

The Figure 1.4 above shows plots of expectation values of relevant observables, derived physical quantities and the autocorrelation times (scaled by $\langle C \rangle / L^2$) as they vary with T for different lattice sizes L. These plots summarize the entire critical structure of Ising model tansition.

The average (absolute) magnetization curve as a function of temperature (Fig. 1.4a) is one of the most interesting results of the Ising model. The average (absolute) magnetization is the order parameter for the Ising model which distinguishes the paramagnetic and ferromagnetic phases of the model. As we go to higher and higher lattice sizes, the transition points becomes progressively sharper and shows a clear transition from ferromagnetism ($\langle |m| \rangle \approx 1$) to paramagnetism ($\langle |m| \rangle \approx 0$) after a certain transition temperature T_c at $L = 128$.

Another interesting feature of the Ising phase transitions are the specific heat C_V (Fig. 1.4c) and magnetic susceptibility χ (Fig. 1.4d) curves. They show an approximate divergence at the critical temperature T_c, which becomes exact in the thermodynamic limit $L \to \infty$. Hence, our numerical studies confirm that the Ising phase transition is second-order in nature.

The way to numerically estimate the critical temperature T_c of the phase transition was given by Binder [Binder 1981]. According to Binder, the transition temperature T_c is the temperature at which different U_L curves (corresponding to different lattice sizes L) cross in the thermodynamic limit (Fig. 1.4e). In our studies, we estimated the critical temperature $T_c \approx 2.269$, which is very close to the exact value of $2/\ln\left(1 + \sqrt{2}\right) \approx 2.26918$.

Finally, a short note on autocorrelation times. As one can see in Fig. 1.4f, we have scaled the τ_{cluster} by $\langle C \rangle / L^2$, where $\langle C \rangle$ is the average cluster size. We claim that this is the correct autocorrelation time to compare with the Metropolis autocorrelation times [Tamayo et al]. This is because N Metropolis sweeps are fundamentally different than N Wolff sweeps. If we go through N sweeps,

$$\text{For Metropolis} \; \longrightarrow N \cdot L^2 \; \text{spin flips}$$
$$\text{For Wolff cluster} \; \longrightarrow N \cdot \langle C \rangle \; \text{spin flips}$$

So if we were to define an equivalent unit of time as $(\# \text{ of spin flips})/L^2$, then for N sweeps

$$T_{\text{Metro}} = \frac{N \cdot L^2}{L^2} = N$$
$$T_{\text{Wolff}} = N \frac{\langle C \rangle}{L^2}$$

Hence, we also scale our Wolff autocorrelation time τ_{cluster} by a factor of $\langle C \rangle / L^2$, and we can see in Fig. 1.4f that it's much more efficient compared to the Metropolis algorithm (Fig. 1.3b). Further, the autocorrelation times are observed to scale with system size as a power law

$$\tau_{\text{int}} \sim L^z$$

where z is the dynamical critical exponent, and can be used to quantify the efficiency of the algorithm. We will, however, not go in that direction and instead focus on the remaining critical exponents which characterize the Ising phase transition.

1.9 Critical phenomena and Finite-size scaling

We will now give a brief review of critical phenomena and the finite-size scaling properties that can be quantitatively used to study critical properties of the problem using Monte Carlo simulations. In general, phase transitions only happen in the thermodynamic limit ($L\infty$). However, since we only possess finite computational memory and processing time, it is not possible to numerically simulate arbitrarily large system sizes to study the critical properties of a system. Therefore, we use the theory of *finite-size scaling analysis* which uses the results for finite system sizes to deduce conclusions for the thermodynamic limit.

1.9.1 Critical Exponents

The critical phenomena are generally scaling forms that occur near the critical point. For the classical Ising model, we obtain scaling relations for observable expectations near the classical critical point, i.e., the critical temperature T_c. As mentioned earlier, we can use the data from finite-size studies to estimate the critical exponents using the *data-collapse method*. However, this analysis is only possible for second-order phase transitions and it fails for first-order transitions.

The most fundamental concept underlying the theory of critical phenomena is that of a *correlation length*, denoted by ξ. It roughly denotes the typical size of ordered domains in the lattice. Close to the critical point T_c, the correlation length diverges according to a power law

$$\xi \sim t^{-\nu}, \tag{1.9.1}$$

where t is defined as the reduced temperature

$$t \equiv \frac{|T - T_c|}{T_c}, \tag{1.9.2}$$

and ν is one of the critical exponents, and is the same whether we approach T_c from above or below. Similarly, the critical exponent corresponding to the onset of magnetic order is given by β. The order parameter $\langle |m| \rangle$ is zero above T_c, and below T_c it scales as

$$\langle |m| \rangle \sim t^{\beta} \quad (\sim \xi^{-\beta/\nu}) \tag{1.9.3}$$

The susceptibility, as noted previously, diverges at T_c in the thermodynamic limit and scales as

$$\chi \sim t^{-\gamma} \quad (\sim \xi^{\gamma/\nu}) \tag{1.9.4}$$

The specific heat is also diverges from both above and below as it approaches T_c

$$C_V \sim t^{-\alpha} \quad (\sim \xi^{\alpha/\nu}) \tag{1.9.5}$$

It is, however, to be noted that the above scaling relations near the critical point hold true in the infinite size limit ($L \to \infty$). Systems belonging to the same *universality class* have the same set of critical exponents $\{\nu, \beta, \gamma, \delta, \alpha\}$. The universality class does not depend on the microscopic details but instead on the behavior of the system near the critical point.

1.9.2 Finite-size scaling hypothesis

How would the scaling relations modify if the lattice sizes L are finite? The order parameter $\langle |m| \rangle$ does not exactly vanish for $T \geq T_c$, and the divergent quantities (like χ and C_V) saturate to a finite value.

One possible way is to perform finite-size simulations for higher and higher L until the results converge, and extract the critical exponents by estimating the exponent in the power law. However, a much more systematic way is to perform a *finite-size scaling* (FSS) study which uses the regularity in the deviations to extract the critical exponents.

Consider the susceptibility in an infinite size limit which scales as

$$\chi \sim \xi^{\gamma/\nu}$$

Then the *finite-size scaling hypothesis* (which can be proven via renormalization group theory) states that observables close to T_c scale with an additional non-divergent function of ξ/L to account for the deviations in critical behavior at finite sizes

$$\chi(\xi, L) = \xi^{\gamma/\nu} f(\xi/L) \tag{1.9.6}$$

where $f(x) \to$ const. as $x \to 0$ ($L \to \infty$). Since the deviations from the $L \to \infty$ critical behavior occurs when the correlation length ξ is comparable to the system size L, and

the fact that $\xi \sim t^{-\nu}$, we obtain the much more familiar expression of the FSS hypothesis

$$\chi(t, L) = L^{\gamma/\nu}\, g(tL^{1/\nu}) \tag{1.9.7}$$

where g is another scaling function. More generally, for any observable (or derived quantity) Q, the quantity scales as

$$Q(t, L) = L^{\zeta/\nu}\, g_Q(tL^{1/\nu}) \tag{1.9.8}$$

where ζ is the critical exponent corresponding to the scaling of the quantity Q.

$$\textbf{Finite-size scaling relations for 2D Ising model} \tag{1.9.9}$$
$$\begin{aligned}
U_L &= \quad g_U(tL^{1/\nu}) \\
|m| &= L^{-\beta/\nu}\, g_m(tL^{1/\nu}) \\
\chi &= L^{\gamma/\nu}\, g_\chi(tL^{1/\nu}) \\
C_V &= \ln(L)\, g_C(tL^{1/\nu})
\end{aligned}$$

In the case of the 2D Ising model, $\alpha = 0$, and hence the power law scaling doesn't hold. Instead, we have a logarithmic scaling as indicated in the scaling of C_V as shown above.

1.9.3   Data collapse method

Since the master curve $g_Q(x)$ for a quantity Q is an unknown function, one can plot $Q(t, L)\, L^{-\zeta/\nu}$ versus $x = tL^{1/\nu}$ for different sizes to extract the master curve. If the finite-size scaling hypothesis is correct, data for all the different lattice sizes should *collapse* onto each other. However, this would require inputting the correct value of the critical exponents ζ and ν.

Therefore, the problem of *estimating the critical exponents* can be rephrased as a data collapse problem of the observable data $(Q(t, L)\, L^{-\zeta/\nu}$ versus $x = tL^{1/\nu})$ by fine-tuning the exponents ζ and ν. We use the following cost function P_b to as a measure of the collapse, which is essentially a normalized sum of residues, which we get by slightly modifying the cost function given in [1].

$$P_b = \frac{1}{N_{\text{over}}} \sum_p \sum_{j \neq p} \sum_i \frac{\left| L_j^{-\zeta/\nu} Q_{ij} - \varepsilon_p\left(L_j^{1/\nu} t_{ij}\right)\right|}{L_j^{-\zeta/\nu} Q_{ij} + \varepsilon_p\left(L_j^{1/\nu} t_{ij}\right)} \tag{1.9.10}$$

- p indexes the data-set associated to length L_p.

- j also indexes the data-set associated to length L_j, but doesn't include the set p.

- i indexes the data-points inside the set associated to L_j.

- N_{over} is the number of terms we sum over.

- ε_p is the interpolating function based on the values of set p bracketing the argument

in question.

The critical exponents are obtained by minimizing the cost funtion P_b with respect to β, γ, ν

   – $Q = U_L$, minimize $P_b(0, \nu)$ with respect to ν. $\longrightarrow \nu_0$

   – $Q = \langle |m| \rangle$, minimize $P_b(-\beta, \nu_0)$ with respect to β. $\longrightarrow \beta_0$

   – $Q = \chi$, minimize $P_b(\gamma, \nu_0)$ with respect to γ. $\longrightarrow \gamma_0$

The data collapse of the quantities obtained from the Monte Carlo studies is shown in Fig. 1.5. The appropriate fine-tuning of the critical exponents results in an almost perfect collapse of the data near the critical point $t = 0$.
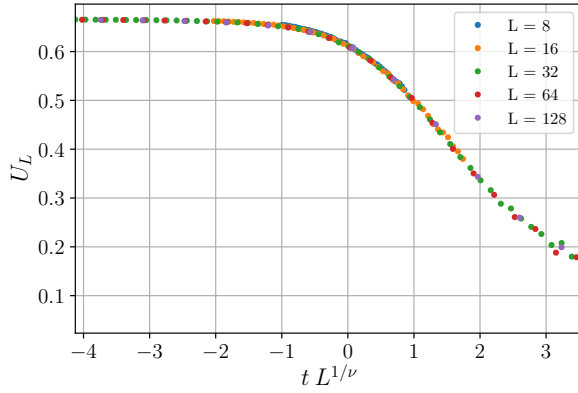
(a) Data collapse for U_L.
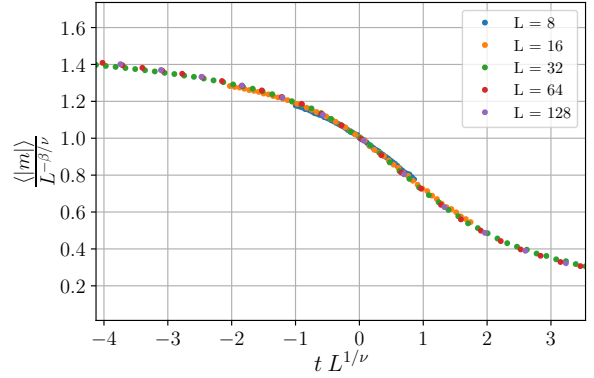
(b) Data collapse for $\langle |m|. \rangle$
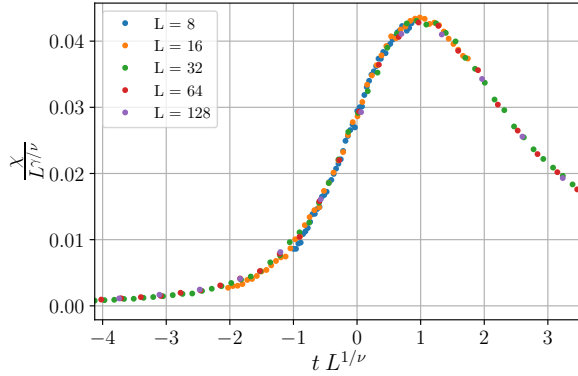
(c) Data collapse for χ.
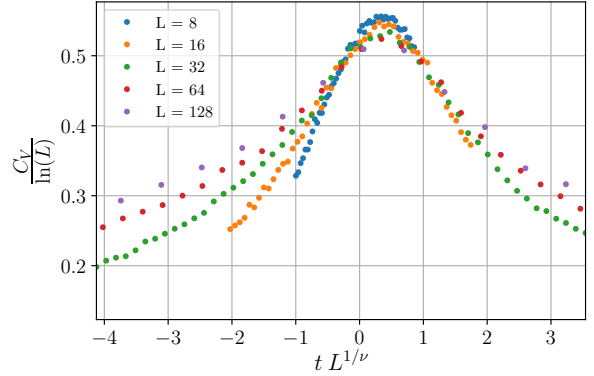
(d) Data collapse for C_V.

Figure 1.5: Data-collapse to extract the critical exponents.

The following table (Table 1.1) summarizes the results of the critical exponents computed from a finite-size scaling study of the data obtained from Monte Carlo simulations compared to the exact values.

Physical Quantity	Exponent	FSS estimate	Exact Value
Specific Heat (C_V)	α	$-$	0
Order Parameter $(\langle|m|\rangle)$	β	0.1204	$1/8$
Magnetic Susceptibility (χ)	γ	1.7301	$7/4$
Correlation Length (ξ)	ν	0.9765	1
Critical Temperature	T_c	2.269	$2/\ln\left(1+\sqrt{2}\right)$

Table 1.1: Summary of critical exponents for the 2D Ising model.

1.10 Summary

In this chapter, we provided a comprehensive introduction for implementing Monte Carlo simulations to classical spin system models. We explicitly discussed the example of the 2D Ising model, constructed both local and cluster update algorithm to compute expectation values of the observables, and described the framework of extracting the critical exponents via finite-size scaling analysis. This methodology can further be extended to other spin models for computing the critical properties near second-order phase transitions. Moreover, in the upcoming chapters, we'll discuss a scheme to generalize this approach to quantum spin models and use *quantum Monte Carlo* methods to explore the critical properties of the quantum phase transition.

2

Semi-classical Monte Carlo for the $J_1 - J_2$ model

The 2-dimensional $J_1 - J_2$ Heisenberg model with nearest (J_1) and next-nearest neighbor (J_2) interactions on a square lattice is an archetypal example of a strongly correlated and frustrated spin model. Although the model is conceptually simple and easy to write down, it exhibits rich and interesting physics owing to the interplay between frustration and quantum fluctuations. The model is known to exhibit two phases with quasi-classical long range antiferromagnetic (AFM) order at $T = 0$ (Fig. 2.1), namely, a Néel-ordered phase ((π, π) AFM) for $J_2/J_1 \lesssim 0.4$, and a stripe-ordered phase (($\pi, 0$) or ($0, \pi$) AFM) for $J_2/J_1 \gtrsim 0.6$. These two AFM states are separated by an intermediate quantum paramagnetic phase ($0.4 \lesssim J_2/J_1 \lesssim 0.6$), also known as the *spin liquid* phase [3]. These phase transitions can be readily studied using state-of-the-art quantum Monte Carlo or exact diagonalization calculations, but these methods require large amounts of computational resources. In this chapter, we will present a semi-classical approach to study the spin-1/2 $J_1 - J_2$ Heisenberg model where we treat a part of the Hamiltonian as a source of *quantum fluctuations* and encode them in a semi-classical manner in combination with classical Monte Carlo simulations, thereby reducing the required computational cost.

2.1 Hamiltonian

With the nearest and the next-nearest neighbor coupling constants being J_1 and J_2, respectively, the Hamiltonian for the quantum spin-1/2 $J_1 - J_2$ Heisenberg model is given by

$$\hat{H} = J_1 \sum_{\langle i,j \rangle} \hat{\vec{S}}_i \cdot \hat{\vec{S}}_j + J_2 \sum_{\langle\langle i,j \rangle\rangle} \hat{\vec{S}}_i \cdot \hat{\vec{S}}_j \tag{2.1.1}$$

where $\langle i, j \rangle$ denotes a nearest neighbor links and $\langle\langle i, j \rangle\rangle$ denotes the next-nearest neighbor links (Fig. 2.2). Further, the spin-1/2 operators are defined as $\hat{\vec{S}} = (\hbar/2)\vec{\sigma}$, and we'll set $\hbar = 1$ for our purposes.

$$\hat{\vec{S}} = \frac{1}{2}\vec{\sigma} \tag{2.1.2}$$

Therefore, in terms of Pauli operators, the Hamiltonian can be written as

(a) Néel-ordered (π, π) AFM   **(b)** Collinear $(\pi, 0)$ AFM
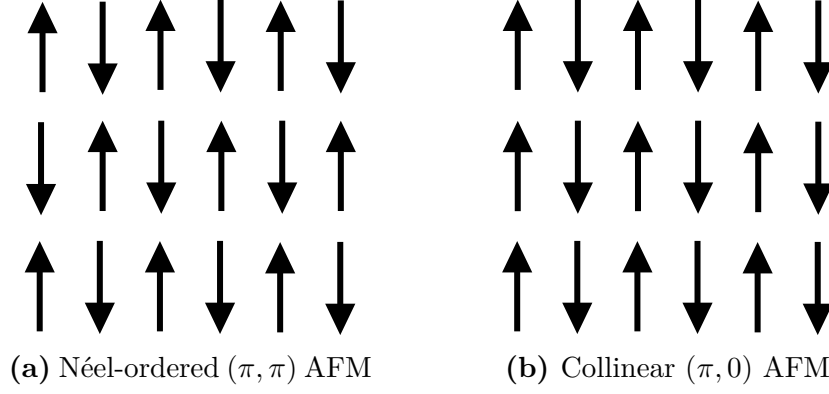
Figure 2.1: Anti-Ferromagnetic phases of the $J_1 - J_2$ Heisenberg Model

$$\hat{H} = \frac{J_1}{4} \sum_{\langle i,j \rangle} \vec{\sigma}_i \cdot \vec{\sigma}_j + \frac{J_2}{4} \sum_{\langle\langle i,j \rangle\rangle} \vec{\sigma}_i \cdot \vec{\sigma}_j \tag{2.1.3}$$

Since the Hamiltonian contains σ^x (or $\hat{X}$), σ^y (or $\hat{Y}$), as well as σ^z (or $\hat{Z}$) terms, the energy eigenstates of the Hamiltonian (consequently, the ground state) will never be an eigenstate of either $\hat{X}, \hat{Y}$ or $\hat{Z}$. Let us look at this statement from another perspective – consider the interaction term

$$\vec{\sigma}_i \cdot \vec{\sigma}_j = \hat{X}_i \hat{X}_j + \hat{Y}_i \hat{Y}_j + \hat{Z}_i \hat{Z}_j \tag{2.1.4}$$

Let's start by considering the $\hat{Z}$ eigenstates $\{|\uparrow\rangle, |\downarrow\rangle\}$. In this basis, the $\hat{Z}_i \hat{Z}_j$ term measures the alignment between sites i and j. On the other hand, the action of the $\hat{X}_i \hat{X}_j$ and $\hat{Y}_i \hat{Y}_j$ is to flip the states (with additional phase factors), hence acting like a *quantum fluctuation*. Therefore, we propose that if we can model an *effective semi-classical* process to simulate the quantum fluctuations in this system, then we can write the interaction term as

$$\vec{\sigma}_i \cdot \vec{\sigma}_j = \hat{Z}_i \hat{Z}_j + \mathcal{E}(Q)_{ij} \tag{2.1.5}$$

where $\mathcal{E}(Q)_{ij}$ is our notation for effective quantum fluctuations between site i and j. We can write our Hamiltonian in a similar fashion

$$\hat{H} = \frac{J_1}{4} \sum_{\langle i,j \rangle} \left[\hat{Z}_i \hat{Z}_j + \mathcal{E}(Q)_{ij} \right] + \frac{J_2}{4} \sum_{\langle\langle i,j \rangle\rangle} \left[\hat{Z}_i \hat{Z}_j + \mathcal{E}(Q)_{ij} \right] \tag{2.1.6}$$

Since we are treating the quantum fluctuations $\mathcal{E}(Q)_{ij}$ in a semi-classical manner, the Hamiltonian (2.1.6) is now diagonal in the $\{|\uparrow\rangle, |\downarrow\rangle\}$ basis just like a classical Ising model. Hence, we can replace $\hat{Z}$ with a classical Ising spin $s_i \in \{\pm 1\}$

$$E = \frac{J_1}{4} \sum_{\langle i,j \rangle} [s_i s_j + \mathcal{E}(Q)_{ij}] + \frac{J_2}{4} \sum_{\langle\langle i,j \rangle\rangle} [s_i s_j + \mathcal{E}(Q)_{ij}] \tag{2.1.7}$$

Therefore, in an effective limit, we propose to simplify the $J_1 - J_2$ Heisenberg model to a **$J_1 - J_2$ classical Ising model with quantum fluctuations** (Eq. (2.1.7)). If
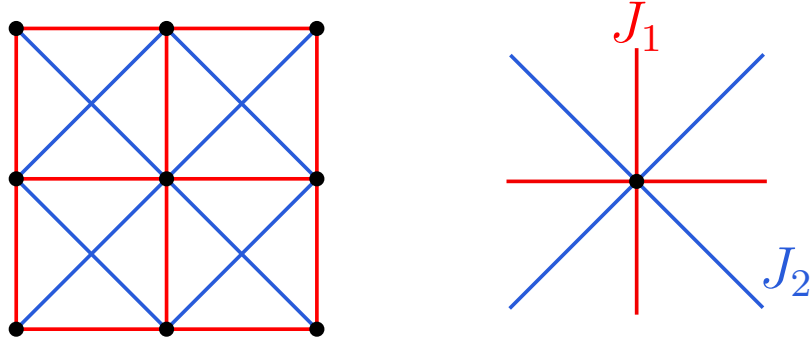
Figure 2.2: $J_1 - J_2$ Heisenberg model lattice structure. The bonds in red represent the J_1 (nearest neighbor) interaction and the bonds in blue represent the J_2 (next-nearest neighbor) interactions.

modelled correctly, these quantum fluctuations should give rise to the same phase diagram as obtained through a thorough Quantum Monte Carlo treatment.

2.2 Quantum fluctuations

To analyze the source of quantum fluctuations in the $J_1 - J_2$ Heisenberg model, we'll start with a simple two-site interaction Hamiltonian. Let's say our two-site Hamiltonian $\hat{h}$ is given by

$$\hat{h} = J\hat{\vec{S}}_i \cdot \hat{\vec{S}}_j \tag{2.2.1}$$

where i and j denote the only two neighboring sites. One can view this as the interaction term appearing in an *addition of angular momentum* problem where $\hat{\vec{M}} = \hat{\vec{S}}_i + \hat{\vec{S}}_j$. Then the interaction term looks like

$$\hat{\vec{S}}_i \cdot \hat{\vec{S}}_j = \frac{\left(\hat{\vec{M}}^2 - \hat{\vec{S}}_i^2 - \hat{\vec{S}}_j^2 \right)}{2} \tag{2.2.2}$$

As can be shown using the Clebsch-Gordan coefficients calculation, the eigenstates of the $\hat{\vec{M}}^2$ and the $\hat{M}_z$ operator are the singlet and triplet states

$$
\left. \begin{aligned}
|s = 1; \, m_s = +1\rangle &= |\uparrow\uparrow\rangle \\
|s = 1; \, m_s = -1\rangle &= |\downarrow\downarrow\rangle \\
|s = 1; \, m_s = 0\rangle &= (|\uparrow\downarrow\rangle + |\downarrow\uparrow\rangle)/\sqrt{2}
\end{aligned} \right\} s = 1 \text{ (triplet)} \tag{2.2.3a}
$$

$$
\left. \begin{aligned}
|s = 0; \, m_s = 0\rangle &= (|\uparrow\downarrow\rangle - |\downarrow\uparrow\rangle)/\sqrt{2}
\end{aligned} \right\} s = 0 \text{ (singlet)} \tag{2.2.3b}
$$

The energy eigenvalues of the singlet and triplet states are accordingly given by

$$\hat{h}\,|s = 1\rangle = \frac{+J}{4}\,|s = 1\rangle \quad \rightarrow \ \text{triplet} \tag{2.2.4a}$$

$$\hat{h}\,|s = 0\rangle = \frac{-3J}{4}\,|s = 0\rangle \quad \rightarrow \ \text{singlet} \tag{2.2.4b}$$

At $T = 0$, the two-site *dimer* state is simply the entangled singlet state $|s = 0;\, m_s = 0\rangle$ with an energy of $-3J/4$. Since entangled singlet dimer states are a purely quantum phenomena, we propose them to be the source of quantum fluctuations at $T = 0$.

However, at finite temperatures $T \neq 0$, the mixed state of the system is described through the thermal density matrix

$$\hat{\rho} = \frac{e^{-\beta\hat{h}}}{\text{Tr}(e^{-\beta\hat{h}})} \tag{2.2.5}$$

Using $\hat{\rho}$, we can compute the thermal expectation value of the energy

$$\langle E \rangle = \frac{\sum_i e^{-\beta E_i} E_i}{\sum_i e^{-\beta E_i}} = \frac{3J}{4}\left(\frac{e^{-\beta J} - 1}{3e^{-\beta J} + 1}\right) \tag{2.2.6}$$

Similarly, we can also compute the expectation value of the net magnetization which corresponds to the operator $\hat{\vec{M}} = \hat{\vec{S}}_i + \hat{\vec{S}}_j$, and it is a straightforward exercise to show that

$$\langle \vec{M} \rangle = 0 \tag{2.2.7}$$

which means that the two-site interaction acts like a *zero magnetization* dimer.

Since the entangled mixed-state (combination of singlet and triplet states) in the two-site Hamiltonian is a purely quantum effect, we can attribute the *quantum fluctuations* in our model to these *dimers*. Further, we propose to model the quantum fluctuations between site i and j as a *semi-classical analog* of dimers

$$\textbf{Semi-classical dimer } \langle \textbf{\textit{i}}, \textbf{\textit{j}} \rangle \rightarrow \quad M(T) = 0, \quad E_J(T) = \frac{3J}{4}\left(\frac{e^{-J/T} - 1}{3e^{-J/T} + 1}\right). \tag{2.2.8}$$

Hence, in addition to the classical Ising spin flip dynamics in our effective model, we have also introduced *dimer* degrees of freedom (to compensate for quantum fluctuations) which can be created or destroyed to minimize the free energy F of the system.

2.3 Analytical results for $T = 0$

Before moving to numerical Monte Carlo simulations to aid our calculations, it is helpful to develop a first-order intuition of the change in physics which occurs by the introduction of semi-classical dimers. Let us consider the $T = 0$ ground state situation. We expect three different type of orders in our system − the Néel-ordered (π, π) AFM phase, the
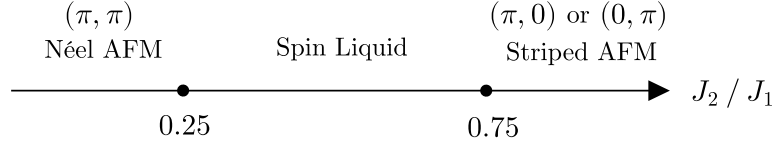
Figure 2.3: Ground State

$(\pi, 0)$ or $(0, \pi)$ AFM phase, and the spin liquid phase (all dimer state). At $T = 0$, the system attains the minimum energy state. Therefore, we can compare the energies (per site) of the three phases to find regions of stability.

For the Néel-ordered (π, π) AFM phase, we have a staggered magnetization along both the axes, and $S_i S_j = -1$ for all the bonds. Therefore, the energy per site is given by

$$E_{(\pi,\pi)} = \frac{J_1}{2}\left(\frac{J_2}{J_1} - 1\right) \tag{2.3.1}$$

Similarly, for the $(\pi, 0)$ or $(0, \pi)$ staggered AFM phase, we have $S_i S_j = -1$ for the next-nearest neighbor links $\langle\langle i, j \rangle\rangle$ and $S_i S_j = \pm 1$ for the nearest neighbours $\langle i, j \rangle$, i.e., keeps fluctuating between ± 1, hence cancelling the contribution.

$$E_{(\pi,0) \text{ or } (0,\pi)} = \frac{J_1}{2}\left(-\frac{J_2}{J_1}\right) \tag{2.3.2}$$

Finally, for the completely dimerized (spin liquid) phase, the energy per site is given by

$$E_{\text{SL}} = \frac{J_1}{2}\left[-\frac{3}{4}(f) - \frac{3}{4}\frac{J_2}{J_1}(1 - f)\right]$$

where f is the fraction of nearest neighbor dimers. Since we are mainly interested in the regime $J_2/J_1 \in [0, 1]$, the parameter value $f = 1$ gives the minimum energy per site

$$E_{\text{SL}} = \frac{J_1}{2}\left(-\frac{3}{4}\right) \tag{2.3.3}$$

Therefore, on comparing the energies, it is straightforward to see that the classical expectation of the phase boundaries at $T = 0$ is given as

$$0 \leq \frac{J_2}{J_1} \leq 0.25 \qquad \longrightarrow \quad (\pi, \pi) \text{ AFM}$$

$$0.25 \leq \frac{J_2}{J_1} \leq 0.75 \qquad \longrightarrow \quad \text{Spin Liquid phase}$$

$$0.75 \leq \frac{J_2}{J_1} \qquad \longrightarrow \quad (\pi, 0) \text{ or } (0, \pi) \text{ AFM}$$

Therefore, **exactly** at $T = 0$, the phase transition in our effective model occurs at the points $J_2/J_1 = 0.25$ and $J_2/J_1 = 0.75$. However, as we'll discuss later, even a small temperature of $T \sim \mathcal{O}(\texttt{1.0e-1})$ can lead to the entropic stabilization of the AFM config-

urations and can play a huge role in shrinking the boundaries of the spin liquid phase to bring the semi-classically derived critical points closer to the quantum results.

2.4 Semi-classical Monte Carlo

Till now, we have proposed two important simplifications of the quantum $J_1 - J_2$ Heisenberg model, i.e.,

1. the quantum model is equivalent to a combination of $J_1 - J_2$ Ising model and some effective quantum fluctuations.

2. the quantum fluctuations can be modelled semi-classically by semi-classical dimers with zero magnetization and a temperature dependent energy $E(T)$ (Eq. (2.2.8)).

To *incorporate* the semi-classical dimers with the $J_1 - J_2$ Ising model, we design a Metropolis Markov chain Monte Carlo algorithm with dimer creation and annihilation steps as Metropolis proposals. Roughly speaking, the Metropolis proposals consist of both spin flips and dimer creation-annihilation steps on the $J_1 - J_2$ Ising lattice, and we expect the effects of the quantum fluctuations to revive in this semi-classical Monte Carlo simulation. A semi-classical Monte Carlo sweep is then defined as follows:

1. Randomly choose a site i on the lattice.

2. Check if the site i is a part of the dimer or a free spin.

3. If site i is a free spin, then we have two possible moves:

   - With a probability p, propose a spin flip $\sigma_i \to -\sigma_i$.

   - With a probability $1 - p$, propose the formation of a semi-classical dimer with another nearest or next-nearest neighbor free spin.

4. If the site i is involved in a dimer (not a free spin), then propose the annihilation of the dimer and create two new random Ising spins.

5. Calculate the change in energy ΔE.

6. Accept the proposed move with a probability of min $\left[e^{-\beta \Delta E}, 1 \right]$.

7. Steps 1 to 6 are then repeated $\mathcal{N} = L^2$ times.

The probability p is changed so as to tune the ratio of random spin-flip dynamics with dimer-formation dynamics. We will discuss the specifics of these parameters in the upcoming sections.

2.5 Dimer dynamics in Monte Carlo

In this section, we will outline the idea behind the physics of creation and annihilation of dimers. The Monte Carlo dynamics is controlled by the change in energies. Hence, it is helpful to calculate the relevant expressions.
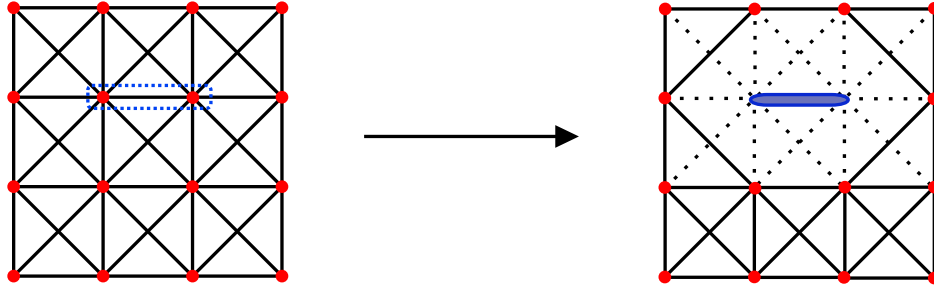
Figure 2.4: Semi-classical dimer formation on $\langle i, j \rangle$ with $S_i = S_j = 0$ and $E = E_J(T)$.

Since the semi-classical dimer is a zero magnetization unit, it implies that the contribution of the neighbor interaction $S_i S_j = 0$ if i or j are part of a dimer. This can be encoded by **setting $S_i = 0$ if site i is making a dimer with one of its neighbors**.

On the basis of this setup, we can calculate the changes in energy in a dimer creation or annihilation process. Let's say a dimer is created between sites $i = (i_x, i_y)$ and $j = (j_x, j_y)$. The change in energy due to dimer creation is then given by

$$
\Delta E_{\mathrm{c}} = + E_J(T) - \frac{J_1}{4} \left[S_{(i_x,i_y)} \sum_{\vec{\delta} \in \{(0,\pm 1),(\pm 1,0)\}} S_{(i_x,i_y)+\vec{\delta}} \quad + S_{(j_x,j_y)} \sum_{\vec{\delta} \in \{(0,\pm 1),(\pm 1,0)\}} S_{(j_x,j_y)+\vec{\delta}} \right]
$$

$$
- \frac{J_2}{4} \left[S_{(i_x,i_y)} \sum_{\vec{\delta} \in \{(1,\pm 1),(-1,\pm 1)\}} S_{(i_x,i_y)+\vec{\delta}} \quad + S_{(j_x,j_y)} \sum_{\vec{\delta} \in \{(1,\pm 1),(-1,\pm 1)\}} S_{(j_x,j_y)+\vec{\delta}} \right] + \frac{J}{4} S_{(i_x,i_y)} S_{(j_x,j_y)}
$$

where J is equal to J_1 or J_2 depending on whether the dimer is formed with the nearest or next-nearest neighbor, respectively, and the Ising spin configuration $\{S_{(x,y)}\}$ is the set of values before the dimer is formed.

Similarly, the change in energy due to annihilation of the dimer between sites i and j and creation of two free spins is given by

$$
\Delta E_{\mathrm{a}} = - E_J(T) + \frac{J_1}{4} \left[S'_{(i_x,i_y)} \sum_{\vec{\delta} \in \{(0,\pm 1),(\pm 1,0)\}} S'_{(i_x,i_y)+\vec{\delta}} \quad + S'_{(j_x,j_y)} \sum_{\vec{\delta} \in \{(0,\pm 1),(\pm 1,0)\}} S'_{(j_x,j_y)+\vec{\delta}} \right]
$$

$$
+ \frac{J_2}{4} \left[S'_{(i_x,i_y)} \sum_{\vec{\delta} \in \{(1,\pm 1),(-1,\pm 1)\}} S'_{(i_x,i_y)+\vec{\delta}} \quad + S'_{(j_x,j_y)} \sum_{\vec{\delta} \in \{(1,\pm 1),(-1,\pm 1)\}} S'_{(j_x,j_y)+\vec{\delta}} \right] - \frac{J}{4} S'_{(i_x,i_y)} S'_{(j_x,j_y)}
$$

where again J is equal to J_1 or J_2 depending on whether it was a nearest or next-nearest neighbor dimer, respectively, and the spin configuration $\{S'_{(x,y)}\}$ is the set of values after the two new random spins are formed in place of the dimer.

2.6 Simulations and results

Now that we have our machinery ready, we implement the Metropolis Monte Carlo algorithm as discussed in Sec. 2.4 with a combination of spin flips and dimer creation/annihilation steps.

We use the following simulation parameters for the semi-classical Monte Carlo simulations of the $J_1 - J_2$ Heisenberg model.

```
lattice size = 10 × 10

J₁ = 4.0
```
$J_2/J_1 \in [0.1, 0.2, \ldots, 1.0]$

$T \in [0.1, 0.2, \ldots, 4.0]$ `(with thermal annealing)`

```
no of equilibration sweeps = 1.0e3

no of sampling sweeps = 5.0e3
```

From preliminary studies, we are aware that the $J_1 - J_2$ Heisenberg model exhibits four different quantum phases $-$ the (π, π) AFM, the spin liquid (quantum paramagnet state), the $(\pi, 0)$ or $(0, \pi)$ AFM, or the thermal paramagnetic phase. Therefore, we require $4 - 1 = 3$ different order parameters to characterize these phases. We define the following three order parameters.

- Staggered magnetizaton (π, π)

$$m_{(\pi,\pi)} = \frac{1}{L^2} \sum_{i=1}^{L^2} (-1)^{i_x + i_y} \, S_i$$

- Staggered magnetizaton $(\pi, 0)$ and $(0, \pi)$

$$m_{(\pi,0)} + m_{(0,\pi)} = \frac{1}{L^2} \sum_{i=1}^{L^2} \left[(-1)^{i_x} + (-1)^{i_y} \right] S_i$$

- Number of dimers

$$N_{\text{dimers}} = N_{J_1 \text{ dimers}} + N_{J_2 \text{ dimers}}$$

Further, we also have the parameter p, which is defined as the ratio of random spin flips to dimer creation steps, which we haven't fixed yet. Since p is a parameter which doesn't explicitly depend upon the model but is an artefact of the design of the algorithm, one needs a way to define what a "good" value of p is. We'll defer this problem to the next section and explore the phase diagrams with different values of p for now.

2.6.1 Phase Diagrams

As can be seen from the phase diagrams, we have all the expected phases emerging from the semi-classical Monte Carlo calculation which are also found from an exact quantum calculation. As a very first step, this shows that it is indeed possible for **quantum phases to emerge by adding quantum fluctuations on top of a classical model.** In fact, the qualitative features of the phase diagram obtained using our semi-classical Monte Carlo approach matches with the essential features of the phase diagram obtained through a cluster mean-field theory calculation of the $J_1 - J_2$ Heisenberg model, as shown in Fig. 2.5.
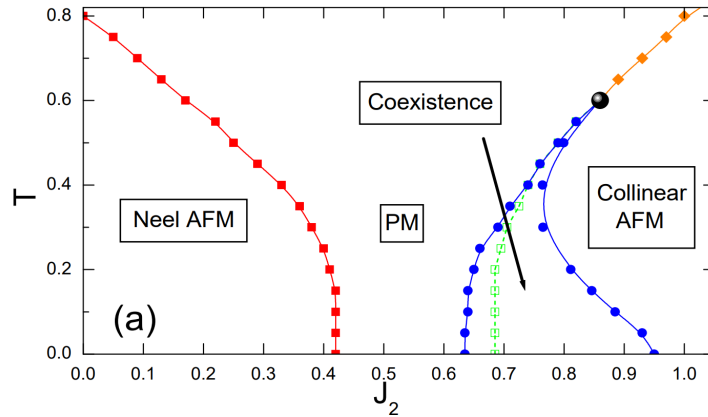
Figure 2.5: Phase diagram of J_1-J_2 model in the $T - J_2$ plane, obtained using 2×2 cluster mean-field theory. Squares with eye guiding line is the second-order Néel-to-paramagnetic phase transition. Solid dots represent coexistence boundaries of paramagnetic phase and collinear AFM phase. The empty squares with dashed line is the actual transition line of equal free energy. The solid dot at ($J_{2c} = 0.86$, $T_c = 0.6$) is the critical point above which the first-order transition changes into a second-order line (diamonds with solid line) [5].

However, as one can notice, the phase boundaries of the Néel AFM to spin liquid, and the spin liquid to the collinear/striped AFM phase transitions does not exactly match with the standard values of $J_2/J_1 \sim 0.4$ and $J_2/J_1 \sim 0.6$, respectively. In fact, the quantum critical points as found from a semi-classical Monte Carlo simulation depends upon the parameter p (and not on the number of sampling sweeps, as expected). The Figures 2.6, 2.7, and 2.8 clearly an increase in the width of the phase boundaries of the spin liquid phase as the value of p is increased. A possible explanation may underline the fact that an increase in the value of p increases the probability of dimer formation which ends up creating a meta-stable fully dimerized state even in the regimes where it is not fully stable. However, as a working definition "correct" value of p can be chosen as the parameter value which maximizes the acceptance rate of the Monte Carlo algorithm.
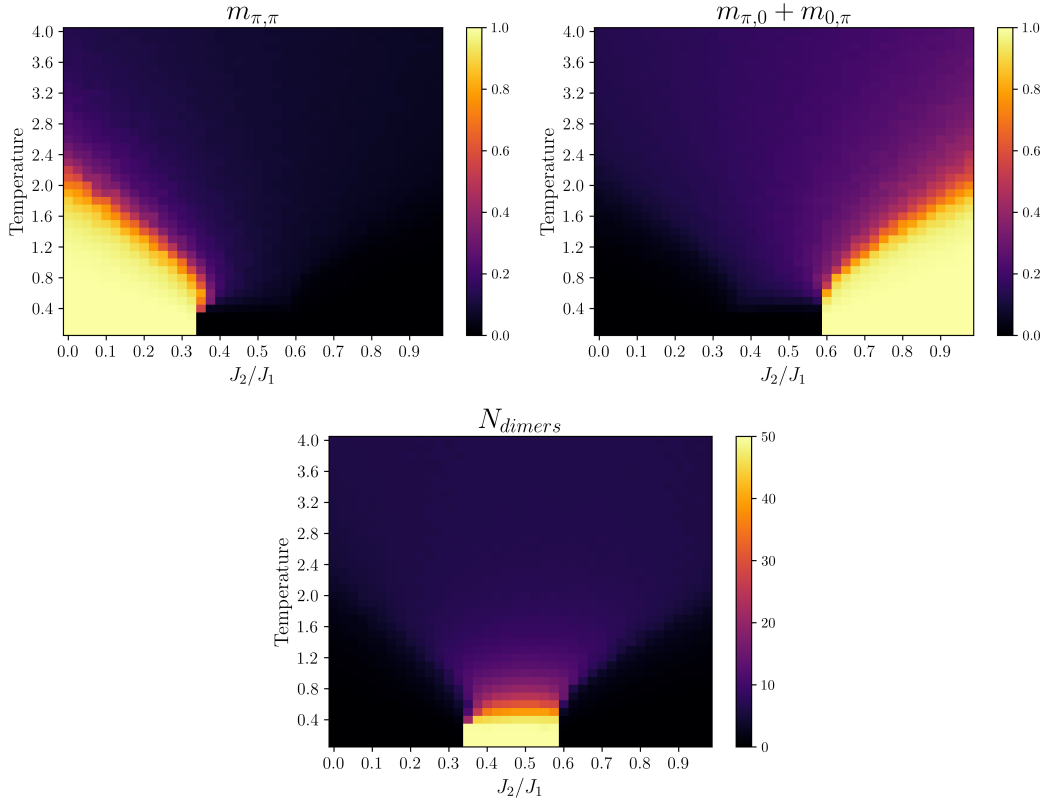
Figure 2.6: Order parameters at $p = 0.15$
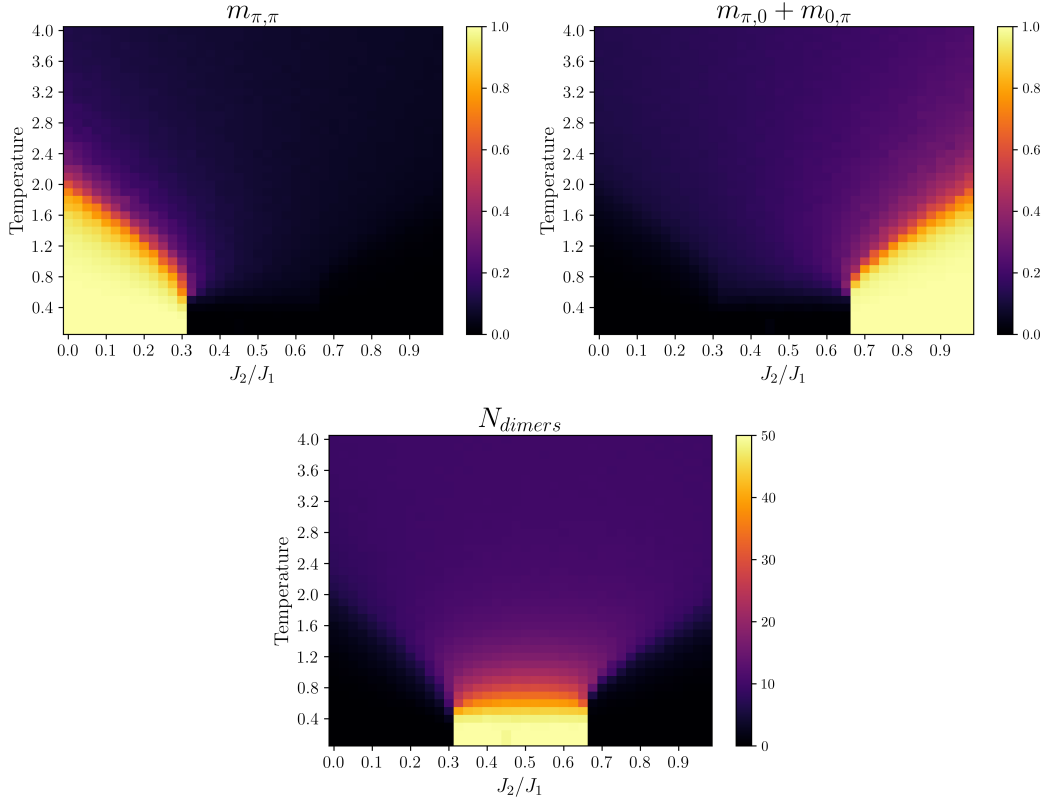
Figure 2.7: Order parameters at $p = 0.25$
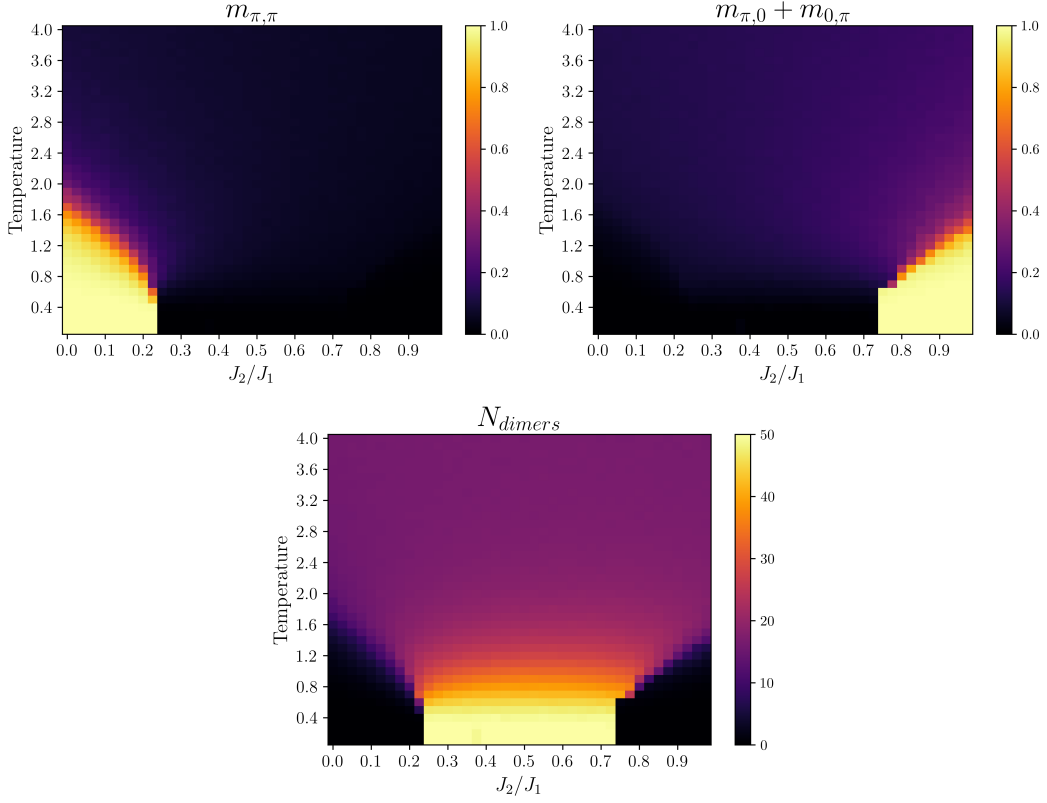
Figure 2.8: Order parameters at $p = 0.50$

2.6.2 Entropic stabilization

As discussed in Section 2.3, we saw that the quantum critical points ($T = 0$) appear at $J_2/J_1 = 0.25$ and $J_2/J_1 = 0.75$ when argued from an energetic viewpoint. However, the spin liquid state is meta-stable only at extremely small temperatures and quickly destabilizes at temperatures of the order $\mathcal{O}(\texttt{1.0e-1})$. This is because the AFM state is entropically more favorable than a dimerized spin liquid state which has a much smaller set of configurations to explore.
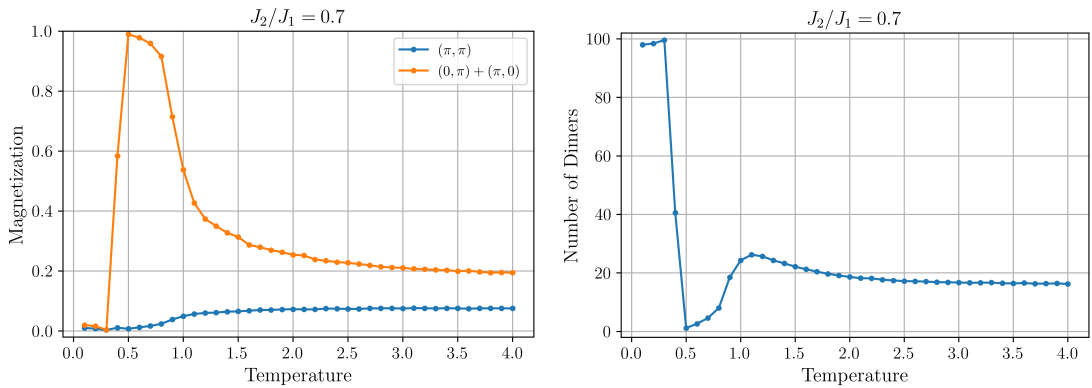
Figure 2.9: Entropic stabilization of AFM and destabilization of the spin liquid state.

 This entropic stabilization process for the AFM state further pushes the boundaries of the phases and can be tuned via the parameter p to give the correct phase transition points. It is, of course, necessary to provide a physical or a mathematical explanation for choosing the value of p which gives the same results as a Quantum Monte Carlo calculation. We aim to address the issue of the correct critical behavior in our future work.

3

$\mathbb{Z}_2$ Lattice Gauge Theory

The principle of gauging symmetries has been one of the most successful paradigms in the history of physics, ranging from the theory of general relativity to the Standard Model of particle physics. Despite the introduction of redundancy, gauging of symmetries is often employed as a guiding principle for constructing physical theories. In condensed matter physics, gauge theories appear as an emergent theory of strongly interacting many-body problems, and gauge description becomes indispensible to understand confined and deconfined phases of matter [2, 4].

In this chapter, we will discuss the simplest gauge theory one can define on a lattice − the pure $\mathbb{Z}_2$ lattice gauge theory (without matter fields) with the topology of a torus (periodic boundary conditions), which was discovered by Franz Wegner in 1971 [7]. We will also discuss the Wegner duality which maps the $\mathbb{Z}_2$ gauge theory to the $\mathbb{Z}_2$ Transverse Field Ising model (TFIM) with the *singlet constraint*. To study the phases of this dual theory, we employ the Path Integral Monte Carlo method which further maps the *d*-dimensional TFIM to a $(d+1)$-dimensional generalized classical Ising model which can be simulated using an extended version of the Metropolis algorithm.

3.1 Hamiltonian

The Hamiltonian of $\mathbb{Z}_2$ gauge theory is given by

$$\hat{H}_{\mathbb{Z}_2} = -J \sum_p \underbrace{\prod_{\ell \in p} \sigma^z_\ell}_{\hat{B}_p} - h \sum_\ell \sigma^x_\ell \tag{3.1.1}$$

where the label ℓ indexes the links/edges on the lattice and the label p denotes a plaquette (square face) on the lattice. As can be seen from Fig. 3.1, the $\hat{B}_p$ term looks like a discrete curl and is the $\mathbb{Z}_2$ analog of magnetic flux through the plaquette p. Similarly, the σ^x_ℓ term is the $\mathbb{Z}_2$ analog of electric flux. This is the simplest Hamiltonian one can construct in terms of gauge invariant $\mathbb{Z}_2$ operators. The gauge transformation of a lattice model is
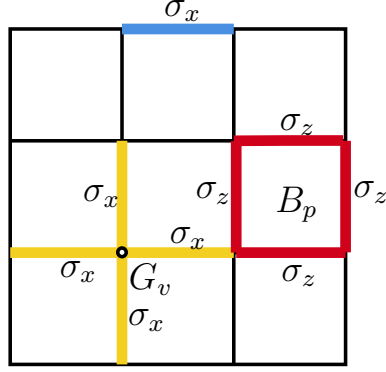
Figure 3.1: $\mathbb{Z}_2$ gauge theory lattice with degrees of freedom living on the links/edges.

given by the local symmetry of the Hamiltonian. For our $\mathbb{Z}_2$ gauge theory Hamiltonian, the gauge transformations are generated by the vertex star operator $\hat{G}_v$.

$$\hat{G}_v \equiv \prod_{\ell \in +} \sigma_\ell^x \tag{3.1.2}$$

By definition, $\hat{G}_v$ is a local symmetry of the Hamiltonian.

$$[\hat{G}_v, \hat{H}] = 0, \quad \forall\, v. \tag{3.1.3}$$

Therefore, G_v is a conserved quantity. Furthermore, since G_v is a $\mathbb{Z}_2$ operator, it squares to identity.

$$\hat{G}_v{}^2 = \mathbb{1} \quad \implies \quad G_v = \pm 1, \quad \forall\, v. \tag{3.1.4}$$

Different eigenvalues of G_v for a vertex v correspond to different sectors of the Hilbert space. Fixing the value of the eigenvalue G_v acts like a gauge-fixing condition. As noted earlier, the σ_ℓ^x term acts like the electric flux analog, i.e., $\sigma_\ell^x \sim e^{iE_\ell}$. This implies that $\hat{G}_v \sim e^{i\nabla \cdot \vec{E}}$. Therefore, the gauge-fixing condition is also commonly known as the "Gauss' law constraint". For the $\mathbb{Z}_2$ Hamiltonian, the Gauss' law constraint can be written as

$$G_v \sim e^{i\pi\rho} = \pm 1, \quad \implies \quad \rho \in \{0, 1\} \tag{3.1.5}$$

Hence, the ± 1 eigenvalues loosely correspond to the absence or the presence of a $\mathbb{Z}_2$ charge on the vertex v, respectively. Since we are interested in probing the low-energy subspace of our problem, we choose the charge-free sector of the Gauss' law constraint

$$\textbf{Constraint 1:}\ G_v = +1, \quad \forall\, v. \tag{3.1.6}$$

Furthermore, as we are interested in probing the topological properties of this model, we invoke periodic boundary conditions in our system. The periodic boundary conditions naturally lead to another constraint between the operators

$$\textbf{Constraint 2:} \quad \prod_p \hat{B}_p = \mathbb{1}. \tag{3.1.7}$$
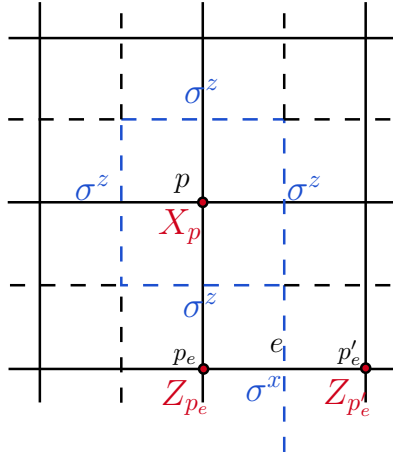
Figure 3.2: Wegner duality mapping of the $\mathbb{Z}_2$ lattice gauge theory to a $\mathbb{Z}_2$ spin (Ising) model. The dotted lines with link gauge variables denotes the original $\mathbb{Z}_2$ gauge theory lattice and the solid lines with vertex spin variables represents the dual lattice.

The product of $\hat{B}_p$ over all the plaquettes creates pair products of σ^z, each of which square identically to $\mathbb{1}$. To study such a gauge theory with constraints is often an extremely non-linear task since a gauge theory, by definition, has redundant unphysical degrees of freedom which are difficult to track numerically.

3.2 Wegner duality

In the context of the $\mathbb{Z}_2$ lattice gauge theory, we map the gauge theory to a spin model via the Wegner duality mapping for the following reasons:

- it eliminates the redundant and unphysical gauge degrees of freedom by mapping it to a spin model with a global $\mathbb{Z}_2$ symmetry. Therefore, there are no local Gauss' law constraints.

- it maps the interacting terms in the $\mathbb{Z}_2$ lattice gauge theory into the non-interacting terms in the $\mathbb{Z}_2$ spin model and vice-versa, resulting in the inversion of the coupling constants.

- it realizes the same algebra between the gauge and spin degrees of freedom.

More precisely, the Wegner duality is defined by the following dual mapping:

$$\sigma_e^x = \sigma_{p_e p_e'}^x \longrightarrow Z_{p_e} Z_{p_e'}, \qquad \prod_{e \, \in \, p} \sigma_e^z = B_p \longrightarrow X_p. \tag{3.2.1}$$

where X_p and Z_p are the new spin degrees of freedom on the dual lattice. Furthermore, as mentioned earlier, they satisfy the same algebra, and it is straightforward to show that

$$X_p^2 = B_p^2 = \mathbb{1}, \qquad \{X_p, Z_p\} = \mathbb{1}, \qquad [X_{p_e}, Z_{p_e'}] = 0 \text{ if } p_e \neq p_e' \tag{3.2.2}$$

The Hilbert space on which X, Z operators act is on a set of spins placed at the centre

of the plaquettes at p. This is also shown in Fig. 3.2 where the $\mathbb{Z}_2$ gauge theory lattice is represented by dotted lines with link degrees of freedom, and the dual lattice is represented by the solid lines with vertex degrees of freedom.

Following the same dual transformation, the dual Hamiltonian becomes

$$\hat{H} = -J \sum_p X_p - h \sum_e Z_{p_e} Z_{p'_e} \tag{3.2.3}$$

which is nothing but the transverse field Ising model (TFIM) with interchanged couplings. However, for the duality to strictly hold, the constraints must also be mapped accordingly. The Gauss' law constraint Eq. (3.1.6) of the original theory is automatically satisfied since

$$\hat{G}_v = \prod_{e \,\in\, +_v} \sigma_e^x = \prod_{\langle p_e, p'_e \rangle \,\in\, \square_v} Z_{p_e} Z_{p'_e} \equiv \mathbb{1} \tag{3.2.4}$$

where the last equality follows because each Z_{p_e} term appears twice. However, the constraint due to periodic boundary conditions isn't trivially satisfied and instead forces

$$\prod_p B_p = \prod_p X_p \overset{!}{=} \mathbb{1} \tag{3.2.5}$$

which is a constraint on the Hilbert space of the dual model, and is known as the **singlet constraint**. We thus conclude that the dual theory is a quantum Ising model (or TFIM) Eq. (3.2.3) with the singlet constraint Eq. (3.2.5).

3.3 Quantum to classical correspondence

The Ising model is one of the simplest spin models studied extensively in condensed matter physics. However, in the presence of a transverse field Eq. (3.2.3) (represented by the X_p operator), the Hamiltonian is not trivially diagonalizable in the Z basis $\{|\uparrow\rangle, |\downarrow\rangle\}$ anymore. Solving this quantum problem directly is somewhat difficult. Therefore, we invoke of the principle of quantum to classical correspondence, which connects the partition functions of the a d-dimensional quantum system to a $d+1$-dimensional classical statistical mechanical system via a path integral approach [6]. The Path Integral Monte Carlo (PIMC) method then uses classical Monte Carlo simulations to calculate the physically relevant quantities of the quantum system.

3.3.1 Imposing the singlet constraint "exactly"

As noted in the previous section, the $\mathbb{Z}_2$ gauge theory with periodic boundary conditions is dual to the singlet Ising model with nearest neighbor interactions,

$$\hat{H} = \underbrace{-J \sum_i X_i}_{H_T} \underbrace{-h \sum_{\langle i, j \rangle} Z_i Z_j}_{H_I}, \qquad \prod_i X_i = \mathbb{1} \tag{3.3.1}$$

where H_I denotes the Ising interaction part, and H_T denotes the transverse field part of the Hamiltonian. Let us first note that

$$\hat{F} \equiv \prod_i X_i \implies \hat{F}^2 = \mathbb{1}. \tag{3.3.2}$$

Thus, we can define the projection operator on the singlet subspace as

$$\hat{P} = \frac{1}{2}(\mathbb{1} + \hat{F}) = \frac{1}{2} \sum_{\mu' \in \{0,1\}} \hat{F}^{\mu'} \tag{3.3.3}$$

The partition function of the singlet Ising model can thus be written as a trace over the singlet-basis states $\{\hat{P}|\{\sigma\}\rangle\}$ where $|\{\sigma\}\rangle = |\sigma_1 \sigma_2 \dots \sigma_{N_x}\rangle$ are the Z-basis product states $\sigma_i \in \{\pm 1\}$.

$$\mathcal{Z} = \text{tr}\, e^{-\beta \hat{H}} = \sum_{\{\sigma\}} \langle\{\sigma\}|\hat{P}\, e^{-\beta \hat{H}}\, \hat{P}|\{\sigma\}\rangle \tag{3.3.4}$$

where $\sum_{\{\sigma\}}$ denotes a sum over all 2^{N_x} different lattice configurations. Further, since $\{\hat{P}|\{\sigma\}\rangle\}$ now form the singlet-basis, their outer products defines the singlet-identity operator $\mathbb{1}_s$,

$$\mathbb{1}_s = \sum_{\{\sigma\}} \hat{P}\,|\{\sigma\}\rangle\, \langle\{\sigma\}|\,\hat{P} = \frac{1}{4} \sum_{\{\sigma\},\mu',\lambda'} \hat{F}^{\lambda'}\,|\{\sigma\}\rangle\, \langle\{\sigma\}|\,\hat{F}^{\mu'} \tag{3.3.5}$$

Since $\hat{F}^{\mu'} = (\prod_i X_i)^{\mu'}$ flips all the spins $\{\sigma\} \longrightarrow \{-\sigma\}$ or leaves them invariant $\{\sigma\} \longrightarrow \{+\sigma\}$ for the cases $\mu' = -1$ and $\mu' = +1$, respectively. Therefore, an alternate representation of its action on the basis states is $\hat{F}^{\mu'}|\{\sigma\}\rangle = |\{\mu\,\sigma\}\rangle$ where $\mu' = (-1)^\mu \implies \mu \in \{\pm 1\}$. The singlet-identity (ignoring the $1/4$ factor) can then be rewritten as

$$\mathbb{1}_s = \sum_{\mu,\, \lambda \in \{\pm 1\}} |\{\lambda\,\sigma\}\rangle\, \langle\{\mu\,\sigma\}| \tag{3.3.6}$$

We will now begin the path integral procedure by slicing the inverse temperature into tiny pieces of width $\Delta\tau$ such that $\beta = N_\tau \Delta\tau$. The Boltzmann exponential factor can then be written as

$$e^{-\beta \hat{H}} = \underbrace{e^{-\Delta\tau \hat{H}}\, e^{-\Delta\tau \hat{H}}\, e^{-\Delta\tau \hat{H}} \dots e^{-\Delta\tau \hat{H}}}_{N_\tau \text{ times}} \tag{3.3.7}$$

and we can insert a singlet-identity between each exponential factor. We will also drop the hats for notational convenience

$$\begin{aligned}
\mathcal{Z} &= \sum_{\{\sigma\},\, \mu,\, \lambda} \langle\{\mu\,\sigma\}|e^{-\beta H}e^{-\beta H} \dots e^{-\beta H}|\{\lambda\,\sigma\}\rangle \\
&= \sum_{\{\sigma_0\},\, \mu_0,\, \lambda_0} \langle\{\mu_0\,\sigma_0\}|e^{-\beta H}\, \mathbb{1}_s\, e^{-\beta H}\, \mathbb{1}_s \dots \mathbb{1}_s\, e^{-\beta H}\, |\{\lambda\,\sigma_0\}\rangle \\
&= \left(\prod_{l=0}^{N_\tau - 1} \sum_{\{\sigma_l\},\mu_l,\lambda_l}\right) \prod_{l=0}^{N_\tau - 1} \langle\{\mu_{l+1}\sigma_{l+1}\}|e^{-\Delta\tau H}|\{\lambda_l\sigma_l\}\rangle
\end{aligned} \tag{3.3.8}$$

where the $2N_\tau$ objects μ_l, λ_l each run over $\{\pm 1\}$, with $\mu_{N_\tau} = \mu_0$, $\lambda_{N_\tau} = \lambda_0$, and $|\{\sigma_{N_\tau}\}\rangle = |\{\sigma_0\}\rangle$. This new index l adds an additional dimension to our problem, and acts like an imaginary time index, with the matrix elements acting like infinitesimal transition amplitudes between imaginary time layers. All the calculations till here have been exact without considering any limits. We now utilize the Trotter product formula to assert that in the limit $N_\tau \to \infty$ or $\Delta\tau \to 0$, the exponential can be decomposed as follows:

$$e^{-\Delta\tau H} = e^{-\Delta\tau(H_I + H_T)} = e^{-\Delta\tau H_I} e^{-\Delta\tau H_T} + \mathcal{O}(\Delta\tau^2) \tag{3.3.9}$$

and we effectively ignore the higher order terms, introducing our first approximation. This approximation gets better as N_τ grows larger. Let us begin by analyzing the matrix elements in the product in Eq. (3.3.8).

$$
\begin{aligned}
\langle\{\mu_{l+1}\sigma_{l+1}\}|e^{-\Delta\tau H}|\{\lambda_l\sigma_l\}\rangle &\approx \langle\{\mu_{l+1}\sigma_{l+1}\}|e^{-\Delta\tau H_T} e^{-\Delta\tau H_I}|\{\lambda_l\sigma_l\}\rangle \\
&= \underbrace{\langle\{\mu_{l+1}\sigma_{l+1}\}|e^{-\Delta\tau H_T}|\{\lambda_l\sigma_l\}\rangle}_{M_{l+1,l}} e^{-\Delta\tau H_I[\{\mu_l\sigma_l\}]}
\end{aligned}
\tag{3.3.10}
$$

where $H_I[\{\mu_l\sigma_l\}]$ is the Ising configuration at the imaginary time layer l

$$
\begin{aligned}
H_I[\{\mu_l\sigma_l\}] &= -h\sum_i \mu_l\sigma_l(i)\mu_l \cdot \sigma_l(i+1) \\
&= -h\sum_i \sigma_l(i)\sigma_l(i+1) = H_I[\{\sigma_l\}]
\end{aligned}
\tag{3.3.11}
$$

since $\mu_l^2 = 1$, and $H_I[\{\sigma_l\}]$ is a classical Ising interaction without any operators. Let us now analyze the leftover matrix element $M_{l+1,l}$ in Eq. (3.3.10)

$$
\begin{aligned}
M_{l+1,l} &= \langle\{\mu_{l+1}\sigma_{l+1}\}|e^{-\Delta\tau H_T}|\{\lambda_l\sigma_l\}\rangle = \langle\{\mu_{l+1}\sigma_{l+1}\}|e^{+J\Delta\tau \sum_i X_i}|\{\lambda_l\sigma_l\}\rangle \\
&= \prod_i \langle\mu_{l+1}\sigma_{l+1}(i)|e^{J\Delta\tau X_i}|\lambda_l\sigma_l(i)\rangle \\
&= \prod_i \langle\mu_{l+1}\sigma_{l+1}(i)|\cosh(J\Delta\tau)\mathbb{1} + \sinh(J\Delta\tau)X_i|\lambda_l\sigma_l(i)\rangle \\
&= \prod_i C_l(i)
\end{aligned}
\tag{3.3.12}
$$

The matrix element $C_l(i)$ can further be evaluated as follows: we can write it as an arbitrary function $C_l(i) = A e^{K(\mu_{l+1}\lambda_l\, \sigma_{l+1}(i)\sigma_l(i))}$ where we don't yet know the constants A and K. However, due to the structure of the matrix element,

$$
C_l(i) = \begin{cases} \cosh(J\Delta\tau), & \text{if } \mu_{l+1}\lambda_l\, \sigma_{l+1}(i)\sigma_l(i) = +1 \\ \sinh(J\Delta\tau), & \text{if } \mu_{l+1}\lambda_l\, \sigma_{l+1}(i)\sigma_l(i) = -1 \end{cases}
\tag{3.3.13}
$$

From the postulated form of $C_i(l)$ and Eq. (3.3.13), we can infer that

$$Ae^K = \cosh(J\Delta\tau), \qquad Ae^{-K} = \sinh(J\Delta\tau) \tag{3.3.14}$$

By dividing and multiplying the two equalities above, we obtain the values of the constants

$$A = \sqrt{\frac{1}{2}\sinh(2J\Delta\tau)}, \qquad K = -\frac{1}{2}\ln\tanh(J\Delta\tau) \tag{3.3.15}$$

Therefore, the matrix element $M_{l+1,\,l}$ in Eq. (3.3.12) can be written in the following form

$$M_{l+1,\,l} = A^{N_x}\exp\left[(\mu_{l+1}\lambda_l)\sum_i K\sigma_{l+1}(i)\,\sigma_l(i)\right] \tag{3.3.16}$$

Further, we define

$$Y = h\Delta\tau \tag{3.3.17}$$

Combining eqns. (3.3.16), (3.3.11), and (3.3.8), we can write the partition function as

$$\mathcal{Z} = \left(\prod_{l=0}^{N_\tau-1}\sum_{\{\sigma_l\},\mu_l,\lambda_l}\right)e^{-S'[\sigma,\lambda,\mu]} \tag{3.3.18}$$

where

$$S'[\sigma,\lambda,\mu] = -\sum_l\left[\mu_{l+1}\lambda_l\sum_i K\,\sigma_{l+1}(i)\,\sigma_l(i)\right] - \sum_l\left[\sum_i Y\,\sigma_l(i)\sigma_l(i+1)\right] \tag{3.3.19}$$

The final partition function expression only contains the product $\mu_{l+1}\lambda_l = \xi_l$. Therefore, we can replace sum over $\mu_l,\lambda_l \in \{\pm1\}$ for each l with a sum over $\xi_l \in \{\pm1\}$. Therefore, apart from an overall factor, the partition function looks like

$$\mathcal{Z} = \left(\prod_{l=0}^{N_\tau-1}\sum_{\{\sigma_l\},\,\xi_l}\right)e^{-S'[\sigma,\,\xi]} \tag{3.3.20}$$

where

$$S'[\sigma,\xi] = -\sum_l\xi_l\underbrace{\left[\sum_i K\,\sigma_{l+1}(i)\,\sigma_l(i)\right]}_{H_\tau(l+1,l)} - \sum_l\underbrace{\left[\sum_i Y\,\sigma_l(i)\sigma_l(i+1)\right]}_{H_I(l)}$$
$$= -\sum_l\xi_l\,H_\tau(l+1,l) - \sum_l H_I(l) \tag{3.3.21}$$

If we now write down the partition function and perform a sum over $\xi_l \in \{\pm1\}$ in Eq. (3.3.20),

$$\mathcal{Z} = \prod_{l=0}^{N_\tau-1}\left[\sum_{\{\sigma_l\}}e^{\sum_l H_I(l)}\left(\sum_{\{\xi_l\in\pm1\}}e^{\sum_l\xi_l\,H_\tau(l+1,l)}\right)\right]$$
$$= \prod_{l=0}^{N_\tau-1}\left[\sum_{\{\sigma_l\}}e^{\sum_l H_I(l)}\left(\prod_{l=0}^{N_\tau-1}\left(\sum_{\{\xi_l\in\pm1\}}e^{\xi_l\,H_\tau(l+1,l)}\right)\right)\right]$$
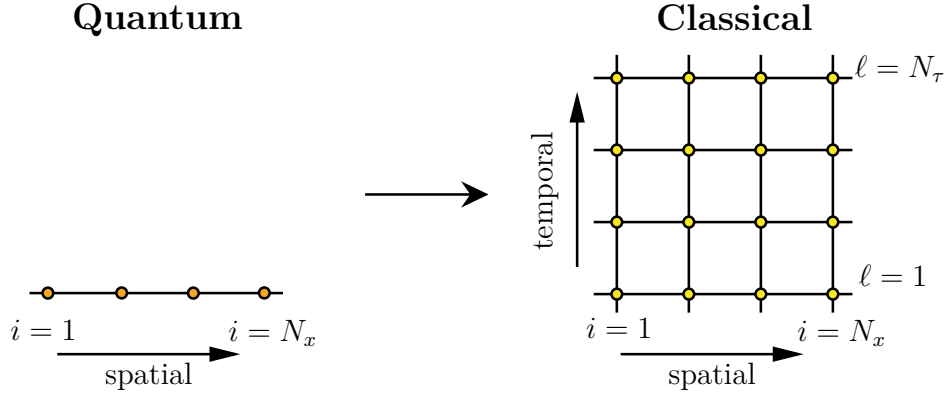
Figure 3.3: Mapping of the $d = 1$ quantum model to a $(d + 1) = (1 + 1)$-dimensional classical Ising model.

$$
= \prod_{l=0}^{N_\tau - 1} \left[\sum_{\{\sigma_l\}} e^{\sum_l H_I(l)} \left(\prod_{l=0}^{N_\tau - 1} \cosh\left(H_\tau(l + 1, l) \right) \right) \right]
$$

$$
= \prod_{l=0}^{N_\tau - 1} \left[\sum_{\{\sigma_l\}} e^{\sum_l H_I(l)} \, e^{\sum_l \ln\cosh\left(H_\tau(l+1,l) \right)} \right]
$$

$$
= \left(\prod_{l=0}^{N_\tau - 1} \sum_{\{\sigma_l\}} \right) e^{-S[\sigma]} \tag{3.3.22}
$$

where the effective classical action (with the singlet constraint imposed) is given by

$$
S[\sigma] = -Y \sum_l \sum_i \sigma_l(i) \, \sigma_l(i + 1) - \sum_l \ln\cosh\left[K \sum_i \sigma_{l+1}(i) \, \sigma_l(i) \right] \tag{3.3.23}
$$

If we start with a d-dimensional quantum Ising model, the quantum to classical correspondence maps it to a $d + 1$-dimensional generalized classical Ising model, where the spatial interactions contains standard pairwise terms $\sim \sigma_l(i) \, \sigma_l(i)$, but the layer interactions are governed by a $\sim \ln\cosh(\sigma_{l+1}(i) \, \sigma_l(i))$. This classical model can then be simulated using the classical Metropolis Monte Carlo algorithm. For the purposes of this thesis, we will be studying the classical analog of the singlet Ising model (Eq. (3.3.23)) in $(1 + 1)d$ and the relevant physical observables using Monte Carlo simulations.

3.3.2 Alignment observable and the subsystem symmetry

Let us begin by looking at a particularly interesting local observable which appears inside the ln cosh term in the classical action Eq. (3.3.23). We call this observable as the alignment observable

$$
A(l) \equiv \frac{1}{N_x} \sum_{i=0}^{N_x - 1} \sigma_i(l) \sigma_i(l + 1) = \frac{1}{N_x} (N_a(l) - N_o(l)) \tag{3.3.24}
$$
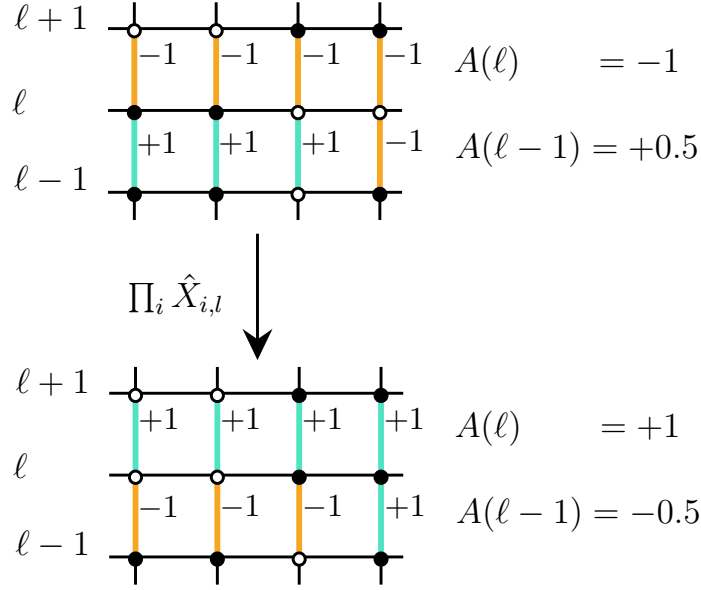
Figure 3.4: The action of the alignment flip operation $\hat{F}(l)$ on the individual spins and the alignment observable $A(l)$. The blue links denote an aligned pair, and the orange links denote an oppositely aligned pair. The links flip on the application of $\hat{F}(l)$, also flipping the value of $A(l)$ and $A(l-1)$.

where N_a denotes the number of aligned pairs and N_o denotes the number of oppositely aligned pairs. This observable effectively measures the *alignment* between the spins of layers l and $l+1$. In terms of the local alignment observables, the classical action for a $(1+1)$-dimensional classical model can be rewritten as

$$S[\sigma] = -Y \sum_{l=0}^{N_\tau - 1} \sum_{i=0}^{N_x - 1} \sigma_l(i)\,\sigma_l(i+1) - \sum_{l=0}^{N_\tau - 1} \ln \cosh\left[K N_x A(l)\right] \tag{3.3.25}$$

The alignment observable transforms in a special way under a transformation, which makes it worth tracking.

Consider a transformation which flips the spins along a particular layer l. Although we aren't formally working with quantum objects right now, we can still define the transformation via a local "operator"

$$\hat{F}(l) \equiv \prod_{i=0}^{N_x - 1} \hat{X}_{i,\,l} \tag{3.3.26}$$

where the $\hat{X}_{i,\,l}$ flips the classical spin variables $\sigma_l(i) \longrightarrow -\sigma_l(i)$. Since it only flips the spins along the layer l,

$$A(l) \longrightarrow \frac{1}{N_x} \sum_{i=0}^{N_x - 1} [-\sigma_i(l)]\sigma_i(l+1) = -A(l)$$

$$A(l-1) \longrightarrow \frac{1}{N_x} \sum_{i=0}^{N_x - 1} \sigma_i(l-1)[-\sigma_i(l)] = -A(l-1) \tag{3.3.27}$$

it flips the alignments of the layers l and $l-1$ (Fig. 3.4). Therefore, it's also commonly referred to as an *alignment flip* operation. However, the classical action (Eq. (3.3.25)) contains terms which remain agnostic under the above transformation

- Spatial interaction: $[-\sigma_l(i)][-\sigma_l(i+1)] = \sigma_l(i)\,\sigma_l(i+1)$.

- Temporal interaction: $\ln\cosh[KN_x(-A(l))] = \ln\cosh[KN_xA(l)]$

Therefore, the action remains invariant under the alignment flip operator,

$$S[\sigma] \xrightarrow{\text{Alignment Flip } \hat{F}(l)} S[\sigma] \tag{3.3.28}$$

and the alignment flip operator $\hat{F}(l)$ is referred to as a *subsystem symmetry.*

This also implies that configuration space states with positive and negative values of the alignment observable would be equally probable in a stochastic simulation such as Monte Carlo. Therefore, on average, $\langle A(l)\rangle \overset{!}{=} 0 \ \forall\, l$, and this quantity can be used as a proxy for ensuring that our effective classical model is indeed simulating the singlet constrained physics of the quantum model.

3.4 Naive Metropolis Monte Carlo simulations

In this section, we will discuss a direct Metropolis Monte Carlo implementation of the $(1+1)d$ generalized classical Ising model in Eq. (3.3.25). We have already outlined the major details of the Metropolis algorithm in Chapter 1. The Metropolis algorithm only consists of spin flip proposals on the $(1+1)d$ lattice. As we'll see later, this straightforward but naive implementation doesn't give the correct equilibration behavior and doesn't simulate the correct physics of the problem.

In quantum Monte Carlo simulations such as these, we usually keep $\Delta\tau = 1$, i.e. $\beta = N_\tau$, and the ground state properties of the system are studied by making the number of sites on the imaginary time axes as large as possible $N_\tau \to \infty$. As mentioned in the last section, we are particularly interested in tracking the Monte Carlo average of the alignment observables which act as an indicator of a good simulation. We perform the simulation over increasing lattice sizes N_x and an increasing number of Monte Carlo sweeps to understand the dependence on the simulation results on these parameters.

For the simulations, we use the following parameters

`spatial lattice size` $N_x \in \{2,\ 3,\ 4\ \ldots,\ 20\}$

`no of sampling sweeps` $N_{\text{samp}} \in \{2.0e4,\ 6.0e4,\ 1.0e5,\ \ldots,\ 2.6e5,\ 3.0e5\}$

`imaginary time lattice size` $N_\tau = 40, \ \ \Delta\tau = 1.0$

`coupling constants` $K, Y = 1.0$

(a) $\langle A(0) \rangle$ vs N_x
(b) $\langle A(23) \rangle$ vs N_x
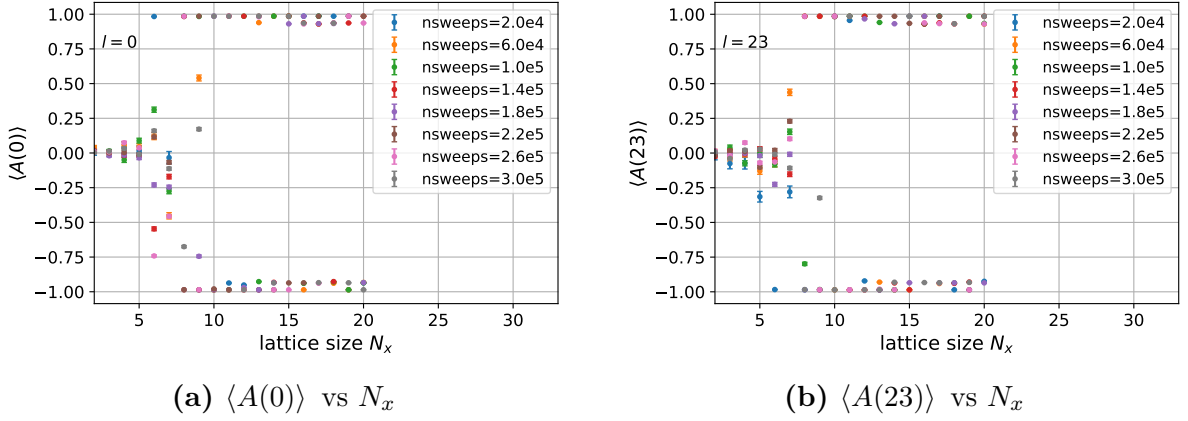
Figure 3.5: $\langle A(l) \rangle$ for different values of l.

3.4.1 Subsystem symmetry breaking

As seen in Fig. 3.5, the results show weak dependence on the number of Monte Carlo sweeps as the system always explores the same region of the configuration space, independent of the number of sweeps. However, above a certain lattice size, i.e., $N_x \sim 10$, the expectation value of the alignment observable gets frozen to ± 1. This effect is independent of the layer chosen as all layers are identical to each other, and is also verified in Fig. 3.6 by plotting the results for two different layers.
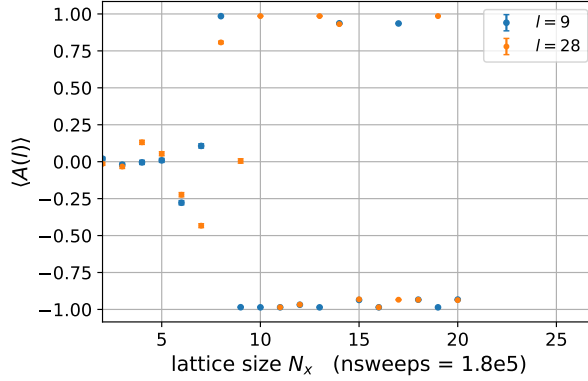
Figure 3.6: $\langle A(l) \rangle$ vs N_x for two different layers $l_1 = 9$, $l_2 = 28$ ran over `nsweeps = 1.8e5`.

The freezing of the alignment value to $\langle A(l) \rangle \neq 0$ indicates that the minima of the action $S[\sigma]$ gets extremely deep on the opposite sides of the configuration space which leads to a high energy barrier between the $A(l) = -1$ and $A(l) = +1$ sides of the configuration space.

The breaking of this subsystem symmetry gives us the first indication that a naive implementation of the Metropolis algorithm cannot give us the correct equilibration behavior of this system.

3.4.2 Autocorrelation function

Another quantity which is shown to give undesired results with the onset of subsystem symmetry breaking is the autocorrelation function of the alignment observable $A(l)$. For the notational convenience, we briefly switch to writing $A(l)$ as A_l. For the observable A_l, the autocorrelation function is computed as follows

$$\text{Autocorr}[A_l] = \frac{\langle A_l(k) A_l(k+T) \rangle}{\langle A_l(k)^2 \rangle} = \frac{1}{N-T} \sum_{k=0}^{N-T-1} \frac{A_l(k) \cdot A_l(k+T)}{\langle A_l(k)^2 \rangle} \tag{3.4.1}$$

where the average is taken over the first $N - T$ measurements, i.e.

$$\langle A_l(k)^2 \rangle = \frac{1}{N-T} \sum_{k=0}^{N-T-1} [A(k)]^2 \tag{3.4.2}$$

One might notice that this definition of autocorrelation function looks slightly different. This is because we have forced $\langle A_l \rangle = 0$, since that is the general expectation when the desired subsystem symmetry is present in the system. If we don't force $\langle A_l \rangle = 0$, we would obtain autocorrelation values for the system oscillating in one of the minima wells, which is an undesirable quantity for us.

In the following simulation, we have set `nsweeps = 2.0e4`, $N_x = 20$, $N_\tau = 40$, $\Delta\tau = 1.0$, and the autocorrelations are computed for $T \in \{$ `1, 2, ..., 3000` $\}$.
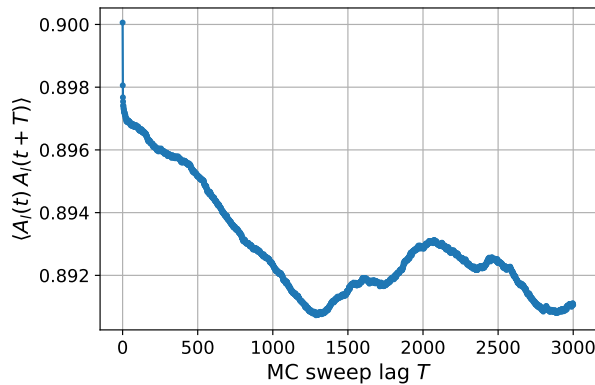
Figure 3.7: Autocorrelation function $\langle A_l(k) A_l(k+T) \rangle$.

In Fig. 3.7, we see that the autocorrelation function stays nearly constant ≈ 0.89 even for $T = 3000$, which implies that autocorrelation time $\tau \to \infty$ for the observables $A(l)$. Hence, once the system gets stuck in one of the $A(l) \pm 1$ minima wells, it almost never gets the chance to escape to the other side of the configuration space.

Therefore, a naive Metropolis algorithm implementation with single spin flips to govern the Monte Carlo dynamics is not sufficient to simulate our effective classical system with subsystem symmetries (which is a direct consequence of the singlet constraint).

3.5   Restoring the subsystem symmetry

In the previous section, we were able to conclusively arrive at the fact that single spin flip Metropolis Monte Carlo simulations are insufficient for exploring the $(1+1)d$ generalized classical Ising model. Due to the freezing of the alignment measurements, the Markov chain describing the single spin flip Metropolis simulation is found to not be ergodic.

This type of a symmetry breaking also occurs in the classical $\mathbb{Z}_2$ Ising model (without any $\ln \cosh$ terms), where the ferromagnetic phase appears as a $\mathbb{Z}_2$ symmetry-broken phase and describes the actual physics instead of being a problem. However, in our case, subsystem symmetry breaking is an obstacle and its preservation is crucial since we want our original quantum model to remain in the singlet sector of the Hilbert space.

3.5.1   Alignment flips as Metropolis proposal moves

The root cause of subsystem symmetry breaking is the inability of the standard Metropolis Monte Carlo to explore the entire configuration space. This is because the two equally accessible regions have a strong energy barrier between them, preventing states of positive (negative) alignment to tunnel to states of negative (positive) alignment.

One of the possible ways to restore this symmetry is by utilizing the special properties of the alignment flip operation Eq. (3.3.26) defined in Section 3.3.2. The alignment flip operation fixes the problem of alignment freezing by forcefully flipping the alignment of a layer, thereby introducing a new channel for connecting positively and negatively aligned regions of the configuration space which was previously inaccessible.

Another interesting feature of the alignment flip operation is that it leaves the effective classical action $S[\sigma]$ invariant Eq. (3.3.28). As a consequence, if the alignment flip operation is introduced as a Metropolis proposal move, then it is an always accepted move since $\Delta S = 0$ always. Therefore, we *propose* that the *modified Metropolis algorithm* is a combination of both random spin flip proposals as well as random alignment flip operations. More precisely, a single Monte Carlo sweep of this modified algorithm is defined as follows,

- $N_x N_\tau$ random spin flip proposals on the $(1+1)d$ lattice.
- $\lfloor N_\tau / f \rfloor$ random alignment flips.

where $f \in \mathbb{R}^+$ tunes the ratio of number of random alignment flips to the number of random spin flip proposals. We expect small values of $f \sim \mathcal{O}(1)$ should be enough to restore the subsystem symmetry in our simulations.

3.5.2   Algorithm

We will now discuss an algorithmic implementation by including both random alignment flip and random spin flip proposals into the Monte Carlo simulation, i.e., $f N_x$ random spin flip proposals followed by one random alignment flip.

algorithm singlet-metropolis
begin
   define $\sigma[N_x, N_\tau]$;
   initialize spins $\sigma[i, l]$;
   define weighted alignment array $\varepsilon[N_\tau]$;
   initialize $\varepsilon[l] = \sum_i K_i \sigma_i(l+1)\sigma_i(l), \quad \forall\, l$;
   // Metropolis updates
   for $n \in \{1, 2, \ldots N_{\mathrm{samp}}\}$
   begin
      // Single Monte Carlo step
      for $m \in \{1, 2, \ldots N_x \cdot N_\tau\}$
      begin
         // Random spin flip proposal
         choose site (random, sequential) := (i_0, l_0);
         define $\varepsilon'_{l_0}, \; \varepsilon'_{l_0-1}$;
         define $\Delta S, \; \Delta S_x, \; \Delta S_t$;

         $\varepsilon'_{l_0-1} = \varepsilon[l_0 - 1] + 2K_{i_0} \cdot \sigma(i_0, l_0) \cdot \sigma(i_0, l_0 - 1)$;
         $\varepsilon'_{l_0} \quad = \varepsilon[l_0] \qquad + 2K_{i_0} \cdot \sigma(i_0, l_0) \cdot \sigma(i_0, l_0 + 1)$;

         $\Delta S_x = 2\Delta\tau \cdot h_{i_0} \cdot \sigma(i_0, l_0) \cdot [\sigma(i_0 - 1, l_0) + \sigma(i_0 + 1, l_0)]$;
         $\Delta S_t = \ln\left[\cosh(\varepsilon[l_0])/\cosh\left(\varepsilon'_{l_0}\right)\right] + \ln\left[\cosh(\varepsilon[l_0 - 1])/\cosh\left(\varepsilon'_{l_0-1}\right)\right]$;
         $\Delta S = \Delta S_x + \Delta S_t$;

         define $p =$ random number;
         if $p < \exp(-\Delta S)$
         begin
            $\varepsilon[l_0 - 1] = \varepsilon'_{l_0-1}$;
            $\varepsilon[l_0] \qquad = \varepsilon'_{l_0}$;
            $\sigma[i_0, l_0] = (-1) \cdot \sigma[i_0, l_0]$;
         end

         // Random alignment flip moves
         if m % fN_x==0
         begin
            choose random layer := l
            for $i \in \{1, 2, \ldots N_x\}$
            begin
               $\sigma[i, l] = (-1) \cdot \sigma[i, l]$;
            end
            $\varepsilon[l - 1] = -\varepsilon[l - 1]$;
            $\varepsilon[l] \qquad = -\varepsilon[l]$;
         end

```
        end
    end
end
```

We implement the above algorithm in `C++` and parallelize it using the `mpi4py` package in `Python`.

3.5.3   Results with alignment flips

This section reviews the results obtained from the singlet Metropolis Monte Carlo simulation with alignment and spin flip moves.
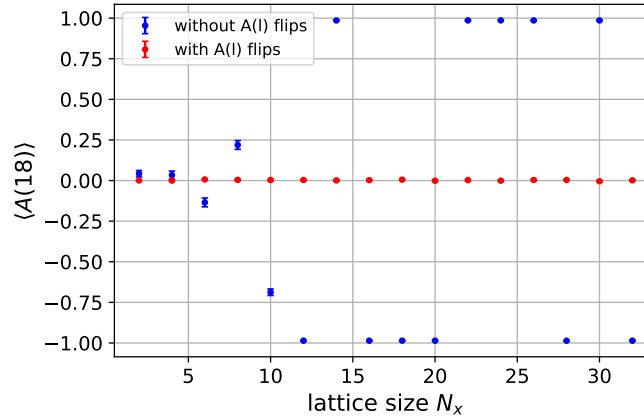
Simulation parameters

    alignment flip fraction $f = 2.0$

    spatial lattice size $N_x \in \{2, 4, 6 \ldots, 32\}$

    no of sampling sweeps $N_{\text{samp}} = 5.0e4$

    imaginary time lattice size $N_\tau = 40, \quad \Delta\tau = 1.0$

    coupling constants $K, Y = 1.0$

The simulations are performed both with and without alignment flips and the results of the expectation values of $A(l)$ are contrasted in Fig. 3.8. As proposed, the introduction

Figure 3.8: $\langle A(l = 18) \rangle$ both with and without alignment flips for different N_x.

of alignment flip proposals to the Metropolis algorithm makes the configuration space equally accessible in both positive and negative alignment regions. This leads to the $\langle A(l) \rangle \approx 0$ for all spatial lattice sizes, hence fixing the subsystem symmetry breaking.

This is also demonstrated in Fig. 3.9 where the Metropolis algorithm is shown to traverse both $A(l) > 0$ and $A(l) < 0$ regions of the configuration space. This verifies that ergodicity is indeed restored and the subsystem symmetry of the generalized classical Ising model is preserved.
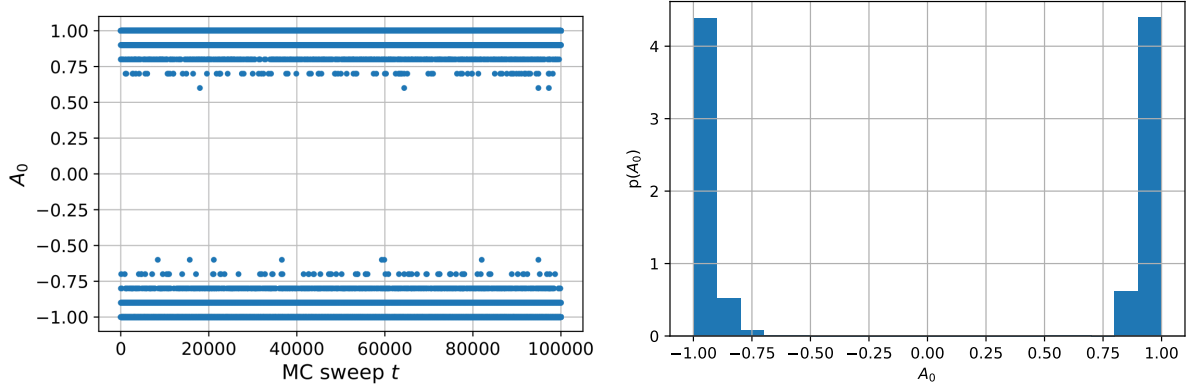
(a) $A(l)$ measurements vs MC time.

(b) $A(l)$ measurements histogram.

Figure 3.9: Configuration space exploring both $A(l) > 0$ and $A(l) < 0$ regions with alignment flip moves.

3.5.4 Autocorrelation function

Since the alignment flips fixed the breaking of subsystem symmetry and freezing of the alignment values, we can now use the standard definition of the autocorrelation function

$$\text{Autocorr}[A_l] = \frac{1}{N-T} \sum_{k=0}^{N-T-1} \frac{(A_l(k) - \langle A_l \rangle) \cdot (A_l(k+T) - \langle A_l \rangle}{\langle A_l(k)^2 \rangle} \tag{3.5.1}$$

where the average is taken over the first $N - T$ measurements, i.e.

$$\langle A_l(k)^2 \rangle = \frac{1}{N-T} \sum_{k=0}^{N-T-1} [A(k)]^2 \tag{3.5.2}$$
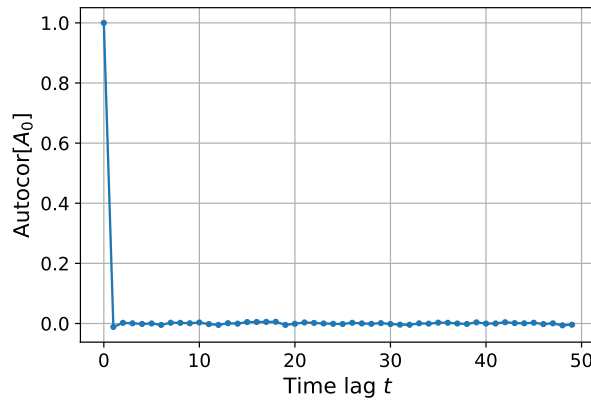
Figure 3.10: Autocorrelation function with alignment flips.

Fig. 3.10 shows that the autocorrelation function drops extremely quickly when the simulation accesses all the allowed regions of the configuration space equally. For this particular simulation, the integrated autocorrelation time was calculated to be $\tau_{\text{int}} \approx 0.529$

implying that the alignment measurements $A(l)$ are highly uncorrelated in the Monte Carlo simulation.

This concludes our verification of the equilibration properties of our singlet Metropolis Monte Carlo algorithm. In the upcoming sections, we'll discuss methods to benchmark our quantum Monte Carlo implementation.

3.6 Benchmarking quantum Monte Carlo

Our previous results lead us to conclude that performing Metropolis Monte Carlo simulations by combining both spin flips and alignment flips keeps the subsystem symmetry of our system intact, and is a reliable way to perform calculations on the $(1+1)d$ generalized classical Ising model, equivalent to the $1d$ singlet Ising model.

However, the applicability of the quantum Monte Carlo calculations can only be verified when compared with analytical or a numerical calculations done directly on the quantum model. Remember that the strength of Monte Carlo simulations lies in the fact that it can work for higher lattice sizes without an exponential overhead in the computational cost. Therefore, the Metropolis Monte Carlo results are benchmarked against direct quantum calculations only for small lattice sizes. This should serve as a check for the pertinency of the quantum Monte Carlo simulations for the singlet Ising model.

3.6.1 Singlet compatible operators

Any operator $\hat{\mathcal{O}}$ defined on the singlet sector of the Hilbert space must satisfy

$$\hat{F}\,\hat{\mathcal{O}}\,\hat{F} \overset{!}{=} \hat{\mathcal{O}} \quad \implies \quad [\hat{F},\,\hat{\mathcal{O}}] \overset{!}{=} 0 \tag{3.6.1}$$

where $\hat{F} = \prod_i \hat{X}_i$ is the global flip operator as defined earlier in Eq. 3.3.2. The above constraint on the operators is a direct consequence of the singlet constraint on the singlet Hilbert space $\mathcal{H}_s$. Mathematically, this can be rephrased as follows - any operator $\mathcal{O}$ defined on $\mathcal{H}_s$ can be written in the outer product notation as

$$\hat{\mathcal{O}} = \sum_{i,\,j} c_{ij}\hat{P}\,|\{\sigma\}\rangle_i\,\langle\{\sigma'\}|_j\,\hat{P} \tag{3.6.2}$$

where $\hat{P} = (\mathbb{1} + \hat{F})/2$ is the singlet projection operator. The action of $\hat{F}$ on $\hat{\mathcal{O}}$ from both sides gives

$$\hat{F}\,\hat{\mathcal{O}}\,\hat{F} = \sum_{ij} c_{ij}\,\underbrace{\hat{F}\hat{P}}_{=\hat{P}}\,|\{\sigma\}\rangle_i\,\langle\{\sigma'\}|_j\,\underbrace{\hat{P}\hat{F}}_{=\hat{P}} = \sum_{i,j} c_{ij}\hat{P}\,|\{\sigma\}\rangle_i\,\langle\{\sigma'\}|_j\,\hat{P} = \hat{\mathcal{O}} \tag{3.6.3}$$

Thus any operator on the singlet sector $\hat{\mathcal{O}} : \mathcal{H}_s \to \mathcal{H}_s$ must satisfy Eq. (3.6.1). The two most elementary observables which satisfy this condition are $\hat{X}_i$ and $\hat{Z}_i\hat{Z}_j$. Such

singlet-compatible quantum operators can then be mapped to their corresponding classical analogs.

3.6.2 Mapping quantum operators to classical observables

As always, the Hamiltonian with the singlet constraint is

$$\hat{H} = -h \sum_i \hat{Z}_i \hat{Z}_j - J \sum_i \hat{X}_i, \qquad \prod_i X_i \stackrel{!}{=} \mathbb{1} \tag{3.6.4}$$

The quantum thermal expectation value of a singlet compatible operator $\hat{\mathcal{O}}$ can then be written as

$$\begin{aligned}
\langle \hat{\mathcal{O}} \rangle &= \frac{\text{Tr}\left(e^{-\beta\hat{H}}\hat{\mathcal{O}}\right)}{\text{Tr}\left(e^{-\beta\hat{H}}\right)} \\
&= \frac{1}{\mathcal{Z}} \sum_{\{\sigma_0\}} \sum_{\mu_0,\lambda_0 \in \{\pm 1\}} \langle \{\mu_0\sigma_0\}|e^{-\Delta\tau\hat{H}}e^{-\Delta\tau\hat{H}} \dots e^{-\Delta\tau\hat{H}}\hat{\mathcal{O}}|\{\lambda_0\sigma_0\}\rangle
\end{aligned} \tag{3.6.5}$$

where we have again traced out the operators in the singlet basis, and sliced the $e^{-\beta\hat{H}}$ into N_τ smaller pieces. Using the cyclic property of trace, we can assert that $\hat{\mathcal{O}}$ does not have to be in the special position at the end of the operator product, therefore

$$\begin{aligned}
\mathcal{Z} \cdot \langle \hat{\mathcal{O}} \rangle = \frac{1}{N_\tau} \Bigg[&\sum_{\{\sigma_0\},\mu_0,\lambda_0} \langle \{\mu_0\sigma_0\}|e^{-\Delta\tau\hat{H}}e^{-\Delta\tau\hat{H}} \dots e^{-\Delta\tau\hat{H}}\hat{\mathcal{O}}|\{\lambda_0\sigma_0\}\rangle \\
&+ \sum_{\{\sigma_0\},\mu_0,\lambda_0} \langle \{\mu_0\sigma_0\}|e^{-\Delta\tau\hat{H}}e^{-\Delta\tau\hat{H}} \dots \hat{\mathcal{O}}e^{-\Delta\tau\hat{H}}|\{\lambda_0\sigma_0\}\rangle \\
&+ \sum_{\{\sigma_0\},\mu_0,\lambda_0} \langle \{\mu_0\sigma_0\}|e^{-\Delta\tau\hat{H}} \dots \hat{\mathcal{O}}e^{-\Delta\tau\hat{H}}e^{-\Delta\tau\hat{H}}|\{\lambda_0\sigma_0\}\rangle \\
\dots &+ \sum_{\{\sigma_0\},\mu_0,\lambda_0} \langle \{\mu_0\sigma_0\}|\hat{\mathcal{O}}e^{-\Delta\tau\hat{H}}e^{-\Delta\tau\hat{H}} \dots e^{-\Delta\tau\hat{H}}|\{\lambda_0\sigma_0\}\rangle \Bigg]
\end{aligned} \tag{3.6.6}$$

Defining $\mu_{N_\tau} = \mu_0$, $\lambda_{N_\tau} = \lambda_0$, and $\{\sigma_{N_\tau}\} = \{\sigma_0\}$, and inserting the singlet identity

$$\mathbb{1}_s = \sum_{\{\sigma_l\},\mu_l,\lambda_l} |\{\lambda_l\sigma_l\}\rangle \langle \{\mu_l\sigma_l\}| \tag{3.6.7}$$

for $l \in \{1, 2, 3 \dots, N_\tau - 1\}$, we get the following expression

$$\begin{aligned}
\mathcal{Z} \cdot \langle \hat{\mathcal{O}} \rangle = \left(\prod_{l=0}^{N_\tau-1} \sum_{\{\sigma_l\},\mu_l,\lambda_l} \right) \frac{1}{N_\tau} \sum_{l_0=0}^{N_\tau-1} \Bigg[&\langle \{\mu_{l_0+1}\sigma_{l_0+1}\}|e^{-\Delta\tau\hat{H}}\hat{\mathcal{O}}|\{\lambda_{l_0}\sigma_{l_0}\}\rangle \\
&\prod_{l \neq l_0} \langle \{\mu_{l+1}\sigma_{l+1}\}|e^{-\Delta\tau\hat{H}}|\{\lambda_l\sigma_l\}\rangle \Bigg]
\end{aligned} \tag{3.6.8}$$

In the following subsections, we perform manipulations on Eq. (3.6.8) for operators $\hat{X}_i$ and $\hat{Z}_i\hat{Z}_j$ to find the analogous classical observables.

Classical analog of $\hat{Z}_i\hat{Z}_j$

The classical analog of the $\hat{Z}_i\hat{Z}_j$ operator is now calculated by substituting $\hat{\mathcal{O}} = \hat{Z}_i\hat{Z}_j$ in Eq. (3.6.8).

$$
\begin{aligned}
\mathcal{Z} \cdot \langle \hat{Z}_i\hat{Z}_j \rangle &= \left(\prod_{l=0}^{N_\tau-1} \sum_{\{\sigma_l\},\mu_l,\lambda_l} \right) \frac{1}{N_\tau} \sum_{l_0=0}^{N_\tau-1} \left[\langle \{\mu_{l_0+1}\sigma_{l_0+1}\}|e^{-\Delta\tau\hat{H}}\hat{Z}_i\hat{Z}_j|\{\lambda_{l_0}\sigma_{l_0}\}\rangle \right. \\
&\qquad\qquad\qquad\qquad\qquad \left. \prod_{l\neq l_0} \langle \{\mu_{l+1}\sigma_{l+1}\}|e^{-\Delta\tau\hat{H}}|\{\lambda_l\sigma_l\}\rangle \right] \\
&= \left(\prod_{l=0}^{N_\tau-1} \sum_{\{\sigma_l\},\mu_l,\lambda_l} \right) \frac{1}{N_\tau} \sum_{l_0=0}^{N_\tau-1} \left[\langle \{\mu_{l_0+1}\sigma_{l_0+1}\}|e^{-\Delta\tau\hat{H}}|\{\lambda_{l_0}\sigma_{l_0}\}\rangle (\lambda_{l_0}\sigma_{l_0}^i)(\lambda_{l_0}\sigma_{l_0}^j) \right. \\
&\qquad\qquad\qquad\qquad\qquad \left. \prod_{l\neq l_0} \langle \{\mu_{l+1}\sigma_{l+1}\}|e^{-\Delta\tau\hat{H}}|\{\lambda_l\sigma_l\}\rangle \right] \\
&= \left(\prod_{l=0}^{N_\tau-1} \sum_{\{\sigma_l\},\mu_l,\lambda_l} \right) \left(\frac{1}{N_\tau} \sum_{l_0=0}^{N_\tau-1} \sigma_{l_0}^i \sigma_{l_0}^j \right) \left[\prod_{l=0}^{N_\tau-1} \langle \{\mu_{l+1}\sigma_{l+1}\}|e^{-\Delta\tau\hat{H}}|\{\lambda_l\sigma_l\}\rangle \right] \quad (3.6.9)
\end{aligned}
$$

where we have used the shorthand notation $\sigma_l(i) \equiv \sigma_l^i$. After performing a few manipulations on the $\prod_l$ product of terms, and performing a sum over $\mu_l, \lambda_l \in \{\pm 1\}$, we obtain a similar discrete path integral as we do for the quantum to classical correspondence of the partition function, over the standard spin basis $\{\sigma_l\}$

$$
\langle \hat{Z}_i\hat{Z}_j \rangle = \frac{1}{\mathcal{Z}} \left(\prod_{l=0}^{N_\tau-1} \sum_{\{\sigma_l\}} \right) \left(\frac{1}{N_\tau} \sum_{l_0=0}^{N_\tau-1} \sigma_{l_0}^i \sigma_{l_0}^j \right) e^{-S[\sigma]} \tag{3.6.10}
$$

where $S[\sigma]$ is the effective classical action of the generalized Ising model Eq. (3.3.23). Therefore, the classical observable corresponding to quantum operator $\hat{Z}_i\hat{Z}_j$ is given by

$$
O_{Z_iZ_j} = \frac{1}{N_\tau} \sum_{l=0}^{N_\tau-1} \sigma_l^i \sigma_l^j \tag{3.6.11}
$$

Classical analog of $\hat{X}_i$

Following a similar procedure as above, we also calculate the classical observable corresponding to $\hat{X}_i$, although the calculation isn't as straightforward here

$$\mathcal{Z} \cdot \langle \hat{X}_i \rangle = \left(\prod_{l=0}^{N_\tau - 1} \sum_{\{\sigma_l\}, \mu_l, \lambda_l} \right) \frac{1}{N_\tau} \sum_{l_0 = 0}^{N_\tau - 1} \left[\langle \{\mu_{l_0+1} \sigma_{l_0+1}\} | e^{-\Delta\tau \hat{H}} \hat{X}_i | \{\lambda_{l_0} \sigma_{l_0}\} \rangle \right.$$

$$\left. \prod_{l \neq l_0} \langle \{\mu_{l+1} \sigma_{l+1}\} | e^{-\Delta\tau \hat{H}} | \{\lambda_l \sigma_l\} \rangle \right] \quad (3.6.12)$$

Let us first analyze the matrix element containing the $\hat{X}_i$

$$\langle \{\mu_{l_0+1} \sigma_{l_0+1}\} | e^{-\Delta\tau \hat{H}} \hat{X}_i | \{\lambda_{l_0} \sigma_{l_0}\} \rangle \approx \langle \{\mu_{l_0+1} \sigma_{l_0+1}\} | e^{-\Delta\tau \hat{H}_I} e^{-\Delta\tau \hat{H}_T} \hat{X}_i | \{\lambda_{l_0} \sigma_{l_0}\} \rangle \quad (3.6.13)$$

The above approximation is valid in the limit $\Delta\tau \to 0$ and $N_\tau \to \infty$. If we make the Ising interaction term $\hat{H}_I$ act on the bra at the left, we get

$$\begin{aligned} \text{Eq. (3.6.13)} &= \langle \{\mu_{l_0+1} \sigma_{l_0+1}\} | e^{-\Delta\tau \hat{H}_T} \hat{X}_i | \{\lambda_{l_0} \sigma_{l_0}\} \rangle \, e^{-\Delta\tau \hat{H}_I(\{\mu_{l_0+1} \sigma_{l_0+1}\})} \\ &= \langle \{\mu_{l_0+1} \sigma_{l_0+1}\} | e^{-\Delta\tau \hat{H}_T} \hat{X}_i | \{\lambda_{l_0} \sigma_{l_0}\} \rangle \, e^{-\Delta\tau \hat{H}_I(\{\sigma_{l_0+1}\})} \\ &= \langle \{\mu_{l_0+1} \sigma_{l_0+1}\} | e^{-\Delta\tau \hat{H}_T} \hat{X}_i | \{\lambda_{l_0} \sigma_{l_0}\} \rangle \, e^{-\Delta\tau \hat{H}_I(\{\sigma_{l_0}\})} \end{aligned} \quad (3.6.14)$$

Ignoring the Ising term for now, we can write $\langle \{\mu_{l_0+1} \sigma_{l_0+1}\} | e^{-\Delta\tau \hat{H}_T} \hat{X}_i | \{\lambda_{l_0} \sigma_{l_0}\} \rangle$ term as follows

$$\begin{aligned} \langle \{\mu_{l_0+1} \sigma_{l_0+1}\} | e^{-\Delta\tau \hat{H}_T} \hat{X}_i | \{\lambda_{l_0} \sigma_{l_0}\} \rangle &= \langle \{\mu_{l_0+1} \sigma_{l_0+1}\} | e^{\Delta\tau \sum_j \hat{X}_j} \hat{X}_i | \{\lambda_{l_0} \sigma_{l_0}\} \rangle \\ &= \left\langle \mu_{l_0+1} \sigma_{l_0+1}^i \left| e^{\Delta\tau \hat{X}_i} \hat{X}_i \right| \lambda_{l_0} \sigma_{l_0}^i \right\rangle \prod_{j \neq i} \left\langle \mu_{l_0+1} \sigma_{l_0+1}^j \left| e^{\Delta\tau \hat{X}_j} \right| \lambda_{l_0} \sigma_{l_0}^j \right\rangle \end{aligned} \quad (3.6.15)$$

The above outer products can be written in a simpler fashion,

$$\begin{aligned} e^{\Delta\tau J \hat{X}_j} &= \cosh(\Delta\tau J) \mathbb{1} + \sinh(\Delta\tau J) \hat{X}_j \\ e^{\Delta\tau J \hat{X}_i} \hat{X}_i &= \sinh(\Delta\tau J) \mathbb{1} + \cosh(\Delta\tau J) \hat{X}_i \end{aligned} \quad (3.6.16)$$

Therefore, when we evaluate the matrix products Eq. (3.6.15), we get

$$\begin{aligned} \left\langle \mu_{l_0+1} \sigma_{l_0+1}^j \left| e^{\Delta\tau \hat{X}_j} \right| \lambda_{l_0} \sigma_{l_0}^j \right\rangle &= A e^{+K \mu_{l_0+1} \lambda_{l_0} \sigma_{l_0+1}^j \sigma_{l_0}^j} \\ \left\langle \mu_{l_0+1} \sigma_{l_0+1}^i \left| e^{\Delta\tau \hat{X}_i} \hat{X}_i \right| \lambda_{l_0} \sigma_{l_0}^i \right\rangle &= A e^{-K \mu_{l_0+1} \lambda_{l_0} \sigma_{l_0+1}^j \sigma_{l_0}^j} \end{aligned} \quad (3.6.17)$$

where $A = \sqrt{\frac{1}{2} \sinh(2J\Delta\tau)}$ and $K = \frac{1}{2} \ln \tanh(J\Delta\tau)$. It is the $\hat{X}$ operator that flips the sign of the factor in the exponential when $j = i$, $l = l_0$. This is key difference in the calculations when compared to $\mathcal{Z}$. Combining Eqs. (3.6.15) and (3.6.17), the matrix product term for the layer l_0 (with $\hat{X}_i$) can be simply written as

$$\langle\{\mu_{l_0+1}\sigma_{l_0+1}\}|e^{-\Delta\tau\hat{H}_T}\hat{X}_i|\{\lambda_{l_0}\sigma_{l_0}\}\rangle = A^{N_x}e^{-K(\mu_{l_0+1}\lambda_{l_0})\sigma^i_{l_0+1}\sigma^i_{l_0}}\prod_{j\neq i}e^{+K(\mu_{l_0+1}\lambda_{l_0})\sigma^j_{l_0+1}\sigma^j_{l_0}}$$

$$= A^{N_x}\exp\left(-2K(\mu_{l_0+1}\lambda_{l_0})\sigma^i_{l_0+1}\sigma^i_{l_0}\right)\exp\left(K(\mu_{l_0+1}\lambda_{l_0})\sum_{j=0}^{N_x-1}\sigma^j_{l_0+1}\sigma^j_{l_0}\right) \quad (3.6.18)$$

For the matrix product associated to all the other layers $l\neq l_0$ (without $\hat{X}_i$), the calculation proceeds similarly and we get

$$\langle\{\mu_{l+1}\sigma_{l+1}\}|e^{-\Delta\tau\hat{H}_T}|\{\lambda_l\sigma_l\}\rangle = A^{N_x}\exp\left(K(\mu_{l+1}\lambda_l)\sum_{j=0}^{N_x-1}\sigma^j_{l+1}\sigma^j_l\right) \quad (3.6.19)$$

Combining the matrix element expressions from both Eqs. (3.6.18) and (3.6.19), we can write the expectation value sum as follows (ignoring the proportionality constants)

$$\mathcal{Z}\cdot\langle\hat{X}_i\rangle = \left(\prod_{l=0}^{N_\tau-1}\sum_{\{\sigma_l\},\mu_l,\lambda_l}\right)\left(\frac{1}{N_\tau}\sum_{l_0=0}^{N_\tau-1}e^{-2K\mu_{l_0+1}\lambda_{l_0}\sigma^i_{l_0}\sigma^i_{l_0+1}}\right)$$
$$\prod_{l=0}^{N_\tau-1}e^{K\mu_{l+1}\lambda_l\sum_j\sigma^j_{l+1}\sigma^j_l + h\Delta\tau\sum_j\sigma^j_l\sigma^{j+1}_l} \quad (3.6.20)$$

Since the expectation value $\langle\hat{X}_i\rangle$ only depends on the product $\mu_{l+1}\lambda_l$, and we are summing over $\lambda_l,\mu_{l+1}\in\{\pm1\}$, we can replace it by just μ_l with the values lying $\in\{\pm1\}$.

$$= \left(\prod_{l=0}^{N_\tau-1}\sum_{\{\sigma_l\}}\right)\frac{1}{N_\tau}\sum_{l_0=0}^{N_\tau-1}\left[\left(\sum_{\mu_{l_0}}e^{K\mu_{l_0+1}\sum_j\sigma^j_{l_0+1}\sigma^j_{l_0}-2K\mu_{l_0+1}\sigma^i_{l_0}\sigma^i_{l_0+1}}\right)e^{h\Delta\tau\sum_j\sigma^j_{l_0}\sigma^{j+1}_{l_0}}\right.$$
$$\left.\prod_{l\neq l_0}\sum_{\mu_l}e^{K\mu_{l+1}\sum_j\sigma^j_{l+1}\sigma^j_l + h\Delta\tau\sum_j\sigma^j_l\sigma^{j+1}_l}\right]$$
$$= \left(\prod_{l=0}^{N_\tau-1}\sum_{\{\sigma_l\}}\right)\frac{1}{N_\tau}\sum_{l_0=0}^{N_\tau-1}\left[\cosh\left(K\sum_j\sigma^j_{l_0+1}\sigma^j_{l_0}-2K\sigma^i_{l_0}\sigma^i_{l_0+1}\right)e^{h\Delta\tau\sum_j\sigma^j_{l_0}\sigma^{j+1}_{l_0}}\right.$$
$$\left.\prod_{l\neq l_0}\cosh\left(K\sum_j\sigma^j_{l+1}\sigma^j_l\right)e^{h\Delta\tau\sum_j\sigma^j_l\sigma^{j+1}_l}\right] \quad (3.6.21)$$

Finally, we can expand the $\cosh(x-y)$ term in Eq. (3.6.21), take out $\cosh\left(K\sum_j\sigma^j_{l_0+1}\sigma^j_{l_0}\right)$ $e^{h\Delta\tau\sum_j\sigma^j_{l_0}\sigma^{j+1}_{l_0}}$ as a common factor, and restore the $\prod_{l\neq l_0}$ to $\prod_{l=0}^{N_\tau-1}$. The product then converts into the usual Boltzmann factor $e^{-S[\sigma]}$ leaving behind the classical observable,

$$\langle \hat{X}_i \rangle = \frac{1}{\mathcal{Z}} \left(\prod_{l=0}^{N_\tau - 1} \sum_{\{\sigma_l\}} \right) \frac{1}{N_\tau} \sum_{l_0=0}^{N_\tau - 1} \left(\cosh\left(2K\sigma_{l_0}^i \sigma_{l_0+1}^i\right) \right.$$

$$\left. - \tanh\left(K \sum_j \sigma_{l_0+1}^j \sigma_{l_0}^j\right) \sinh\left(2K\sigma_{l_0}^i \sigma_{l_0+1}^i\right) \right) e^{-S[\sigma]} \tag{3.6.22}$$

Thus, the extracted classical observable corresponding to the quantum operator $\hat{X}_i$ as

$$O_{X_i} = \frac{1}{N_\tau} \sum_{l=0}^{N_\tau - 1} \left[\cosh\left(2K\sigma_l^i \sigma_{l+1}^i\right) - \tanh\left(K \sum_{j=0}^{N_x - 1} \sigma_{l+1}^j \sigma_l^j\right) \sinh\left(2K\sigma_l^i \sigma_{l+1}^i\right) \right] \tag{3.6.23}$$

Using a few trigonometric identities, it can be written compactly as

$$O_{X_i} = \frac{1}{N_\tau} \sum_{l=0}^{N_\tau - 1} \left[\frac{\cosh\left(2K\sigma_l^i \sigma_{l+1}^i - K\sum_{j=0}^{N_x-1} \sigma_{l+1}^j \sigma_l^j\right)}{\cosh\left(K\sum_{j=0}^{N_x-1} \sigma_{l+1}^j \sigma_l^j\right)} \right] \tag{3.6.24}$$

The central idea surrounding the benchmarking of the quantum Monte Carlo simulations involves comparing the Monte Carlo averages of classical observables O_{X_i} and $O_{Z_i Z_j}$ against the quantum expectation values of quantum operators $\hat{X}_i$ and $\hat{Z}_i \hat{Z}_j$. This is discussed in the following sections.

3.7 The two site problem

The two site problem for the singlet Ising model serves as the simplest non-trivial problem. The two site quantum chain with $N_x = 2$ displays the simplest quantum features of the problem while also being analytically tractable. As the most elementary exercise, it is vital to verify that analytical results for the quantum expectation values of $\hat{X}_i$ and $\hat{Z}_i \hat{Z}_j$ match with the Monte Carlo averages performed for the classical observables O_{X_i} and $O_{Z_i Z_j}$.

3.7.1 Quantum expectation values

For two spin sites, the Hilbert space can be defined to be spanned by the singlet basis

$$\mathcal{H}_s = \text{span}\left\{ \frac{|\uparrow\uparrow\rangle + |\downarrow\downarrow\rangle}{\sqrt{2}}, \frac{|\uparrow\downarrow\rangle + |\downarrow\uparrow\rangle}{\sqrt{2}} \right\} \tag{3.7.1}$$

The above states are labelled as

$$|a\rangle = \frac{|\uparrow\uparrow\rangle + |\downarrow\downarrow\rangle}{\sqrt{2}}, \qquad |b\rangle = \frac{|\uparrow\downarrow\rangle + |\downarrow\uparrow\rangle}{\sqrt{2}} \tag{3.7.2}$$

The expression for the expectation value of an operator is given by

$$\langle \hat{O} \rangle = \text{Tr}\left(e^{-\beta \hat{H}} \hat{O}\right) = \frac{e^{-\beta E_0} \langle w_0 | \hat{O} | w_0 \rangle + e^{-\beta E_1} \langle w_1 | \hat{O} | w_1 \rangle}{e^{-\beta E_0} + e^{-\beta E_1}} \tag{3.7.3}$$

where we have evaluated the trace in the yet-unknown energy eigenbasis. The energy eigenvalues E_i and the eigenvectors $|w_i\rangle$ can be calculated by diagonalizing the Hamiltonian in the singlet basis representation.

$$H := \begin{pmatrix} \langle a | \hat{H} | a \rangle & \langle a | \hat{H} | b \rangle \\ \langle b | \hat{H} | a \rangle & \langle a | \hat{H} | b \rangle \end{pmatrix} \tag{3.7.4}$$

For $N_x = 2$, the quantum Hamiltonian with periodic boundary conditions simplifies to

$$\hat{H} = -2h\hat{Z}_0\hat{Z}_1 - J(\hat{X}_0 + \hat{X}_1) \tag{3.7.5}$$

and after a bit of algebra, the matrix representation in the singlet basis comes out to be

$$H := \begin{pmatrix} -2h & -2J \\ -2J & 2h \end{pmatrix} \tag{3.7.6}$$

Thus, the energy eigenvalues obtained on solving the secular equation gives the following

$$\lambda_\pm = \pm 2\sqrt{h^2 + J^2} \tag{3.7.7}$$

Let us define

$$h = B\cos\theta, \qquad J = B\sin\theta \tag{3.7.8}$$

Then $\lambda_\pm = \pm 2B$, and the $\hat{H}$ matrix becomes

$$H := 2B \begin{pmatrix} -\cos\theta & -\sin\theta \\ -\sin\theta & \cos\theta \end{pmatrix} \tag{3.7.9}$$

To find the eigenvectors, we claim that one of them is given by

$$|w_0\rangle = u\,|a\rangle + v\,|b\rangle \tag{3.7.10}$$

This implies that the other eigenvector must be of the form

$$|w_1\rangle = -v\,|a\rangle + u\,|b\rangle \tag{3.7.11}$$

with u and $v \in \mathbb{R}$ to satisfy the orthonormality relations.

For the eigenvector $|w_0\rangle$ with the eigenvalue $E_0 = -2B$, the matrix equation can be written as follows

$$2B \begin{pmatrix} -\cos\theta & -\sin\theta \\ -\sin\theta & \cos\theta \end{pmatrix} = -2B \begin{pmatrix} u \\ v \end{pmatrix}$$

$$2B \begin{pmatrix} -\cos\theta + 1 & -\sin\theta \\ -\sin\theta & \cos\theta + 1 \end{pmatrix} \begin{pmatrix} u \\ v \end{pmatrix} = \begin{pmatrix} 0 \\ 0 \end{pmatrix}$$

$$2B \begin{pmatrix} 2\sin^2(\theta/2) & -2\sin(\theta/2)\cos(\theta/2) \\ -2\sin(\theta/2)\cos(\theta/2) & 2\cos^2(\theta/2) \end{pmatrix} \begin{pmatrix} u \\ v \end{pmatrix} = \begin{pmatrix} 0 \\ 0 \end{pmatrix} \tag{3.7.12}$$

Solving for u and v, we obtain the relation

$$\sin(\theta/2)u = \cos(\theta/2)v$$
$$\implies u = \cos(\theta/2), \qquad v = \sin(\theta/2) \tag{3.7.13}$$

Let us now calculate the matrix elements $\langle w_i | \hat{O} | w_i \rangle$ for $\hat{O} = \hat{X}_i$, which are used in the evaluation of the thermal expectation value of $\hat{X}_i$.

$$\begin{aligned}
\langle w_0 | \hat{X}_0 | w_0 \rangle &= (\langle a | u + \langle b | v) \hat{X}_i (u | a \rangle + v | b \rangle) \\
&= u^2 \langle a | \underbrace{\hat{X}_0 | a \rangle}_{|b\rangle} + uv \langle a | \underbrace{\hat{X}_0 | b \rangle}_{|a\rangle} + uv \langle b | \underbrace{\hat{X}_0 | a \rangle}_{|b\rangle} + v^2 \langle b | \underbrace{\hat{X}_0 | b \rangle}_{|a\rangle} \\
&= u^2 \langle a | b \rangle + uv \langle a | a \rangle + uv \langle b | b \rangle + v^2 \langle b | a \rangle \\
&= 2uv
\end{aligned} \tag{3.7.14}$$

$$\begin{aligned}
\langle w_1 | \hat{X}_0 | w_1 \rangle &= (- \langle a | v + \langle b | u) \hat{X}_i (-v | a \rangle + u | b \rangle) \\
&= v^2 \langle a | \underbrace{\hat{X}_0 | a \rangle}_{|b\rangle} - uv \langle a | \underbrace{\hat{X}_0 | b \rangle}_{|a\rangle} - uv \langle b | \underbrace{\hat{X}_0 | a \rangle}_{|b\rangle} + u^2 \langle b | \underbrace{\hat{X}_0 | b \rangle}_{|a\rangle} \\
&= v^2 \langle a | b \rangle - uv \langle a | a \rangle - uv \langle b | b \rangle + u^2 \langle b | a \rangle \\
&= -2uv
\end{aligned} \tag{3.7.15}$$

The calculation is exactly similar for $\hat{X}_1$. The expectation value for $\hat{X}$ then evaluates to

$$\langle \hat{X} \rangle = 2uv \left(\frac{e^{2\beta B} - e^{-2\beta B}}{e^{2\beta B} + e^{-2\beta B}} \right) = 2uv \tanh(2\beta B)$$
$$\implies \langle \hat{X} \rangle = \frac{J}{B} \tanh(2\beta B) \tag{3.7.16}$$

The calculation for $\hat{Z}_0 \hat{Z}_1$ is analogous and the matrix elements are evaluated as follows

$$\begin{aligned}
\langle w_0 | \hat{Z}_0 \hat{Z}_1 | w_0 \rangle &= (\langle a | u + \langle b | v) \hat{Z}_0 \hat{Z}_1 (u | a \rangle + v | b \rangle) \\
&= u^2 \langle a | \underbrace{\hat{Z}_0 \hat{Z}_1 | a \rangle}_{|a\rangle} + uv \langle a | \underbrace{\hat{Z}_0 \hat{Z}_1 | b \rangle}_{-|b\rangle} + uv \langle b | \underbrace{\hat{Z}_0 \hat{Z}_1 | a \rangle}_{|a\rangle} + v^2 \langle b | \underbrace{\hat{Z}_0 \hat{Z}_1 | b \rangle}_{-|b\rangle} \\
&= u^2 \langle a | a \rangle - uv \langle a | b \rangle + uv \langle b | a \rangle - v^2 \langle b | b \rangle \\
&= u^2 - v^2
\end{aligned} \tag{3.7.17}$$

$$
\begin{aligned}
\langle w_1 | \hat{Z}_0 \hat{Z}_1 | w_1 \rangle &= (-\langle a| v + \langle b| u) \hat{Z}_0 \hat{Z}_1 (-v |a\rangle + u |b\rangle) \\
&= v^2 \langle a| \underbrace{\hat{Z}_0 \hat{Z}_1 |a\rangle}_{|a\rangle} - uv \langle a| \underbrace{\hat{Z}_0 \hat{Z}_1 |b\rangle}_{-|b\rangle} - uv \langle b| \underbrace{\hat{Z}_0 \hat{Z}_1 |a\rangle}_{|a\rangle} + u^2 \langle b| \underbrace{\hat{Z}_0 \hat{Z}_1 |b\rangle}_{-|b\rangle} \\
&= v^2 \langle a|a\rangle - uv \langle a|b\rangle + uv \langle b|a\rangle - u^2 \langle b|b\rangle \\
&= -(u^2 - v^2)
\end{aligned}
\tag{3.7.18}
$$

Therefore, the expectation value of $\hat{Z}_0 \hat{Z}_1$ evaluates to

$$
\langle \hat{Z}_0 \hat{Z}_1 \rangle = (u^2 - v^2)\left(\frac{e^{2\beta B} - e^{-2\beta B}}{e^{2\beta B} + e^{-2\beta B}} \right) = (u^2 - v^2)\tanh(2\beta B)
$$

$$
\implies \langle \hat{Z}_0 \hat{Z}_1 \rangle = \frac{h}{B}\tanh(2\beta B)
\tag{3.7.19}
$$

3.7.2 Monte Carlo averages

The effective classical action arising out of quantum to classical correspondence looks much simpler for $N_x = 2$

$$
S = -2h\Delta\tau \sum_{l=1}^{N_\tau} \sigma_l^0 \sigma_l^1 - \sum_{l=1}^{N_\tau} \ln\cosh\left[K\left(\sigma_l^0 \sigma_{l+1}^0 + \sigma_l^1 \sigma_{l+1}^1 \right) \right]
\tag{3.7.20}
$$

Thus, for a spin flip $\sigma_{l_0}^{i_0} \to -\sigma_{l_0}^{i_0}$, we can decompose the change in action as

$$
\Delta S_x = 4h\Delta\tau \sigma_{l_0}^0 \sigma_{l_0}^1
$$

$$
\Delta S_\tau = \ln\left[\frac{\cosh\left[K(\sigma_l^0 \sigma_{l+1}^0 + \sigma_l^1 \sigma_{l+1}^1) \right] \cdot \cosh\left[K(\sigma_l^0 \sigma_{l-1}^0 + \sigma_l^1 \sigma_{l-1}^1) \right]}{\cosh\left[K(\sigma_l^0 \sigma_{l+1}^0 - \sigma_l^1 \sigma_{l+1}^1) \right] \cdot \cosh\left[K(\sigma_l^0 \sigma_{l-1}^0 - \sigma_l^1 \sigma_{l-1}^1) \right]} \right]
$$

$$
\Delta S = \Delta S_x + \Delta S_\tau
\tag{3.7.21}
$$

As before, the relevant operators are the mappings of $\hat{X}_i$ and $\hat{Z}_0 \hat{Z}_1$, i.e., the classical observables O_X and $O_{Z_0 Z_1}$ respectively.

$$
O_{Z_0 Z_1} = \frac{1}{N_\tau} \sum_{l=0}^{N_\tau - 1} \sigma_l^0 \sigma_l^1
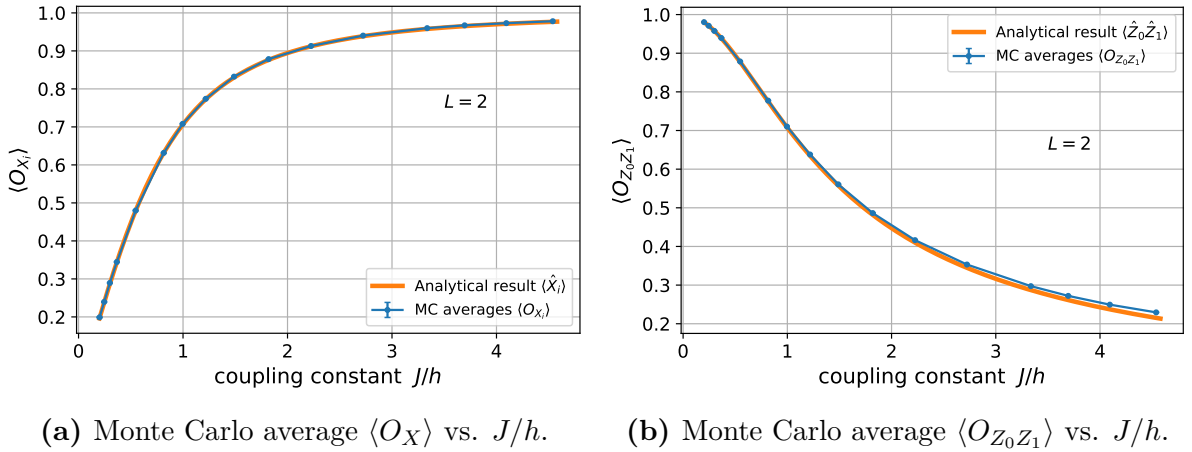\tag{3.7.22}
$$

$$
O_X = O_{X_0} = O_{X_1} = \frac{1}{N_\tau} \sum_{l=0}^{N_\tau - 1} \left[\frac{\cosh\left(K\sigma_l^0 \sigma_{l+1}^0 - K\sigma_l^1 \sigma_{l+1}^1 \right)}{\cosh\left(K\sigma_l^0 \sigma_{l+1}^0 + K\sigma_l^1 \sigma_{l+1}^1 \right)} \right]
\tag{3.7.23}
$$

Finally, we can then use our modified Metropolis Monte Carlo algorithm with spin flips and alignment flips, defined with an acceptance probability of $\min(1, e^{-\Delta S})$. These Monte Carlo averages of O_X and $O_{Z_0 Z_1}$ are then compared against the analytical results for $\langle \hat{X} \rangle$ and $\langle \hat{Z}_0 \hat{Z}_1 \rangle$.

3.7.3 Comparing Monte Carlo against analytical results

We perform the Monte Carlo simulation for $\beta = N_\tau = 50$, keeping $\Delta\tau = 1$ and alignment flip fraction $f = \texttt{1.0}$. However, care needs to be taken while choosing the values of J (consequently K) and h (consequently Y). Since the model only depends on the ratio J/h, we have the freedom of choosing the value of the parameters as large or as small as we want. To explore the system near $J/h = 1$, we have to adjust the parameter values accordingly. If Y is too small, then the values of K near $J/h = 1$ are too large and that results in a low *acceptance rate* and high *trotter error*. The values of K near $J/h = 1$ are small if h is large, but it again results in the same problem. Moreover, disproportionate orders of magnitude of K and Y can lead to spin freezing along one of the directions.

Therefore, we require an optimum range of values for parameters K and Y to explore the system near the $J/h = 1$ point so as to minimize the *trotter error* and maximize the *acceptance rate*. Therefore, we choose $Y = \texttt{0.05}$ and vary K. The $J/h = 1$ then translates $K_* = 1.498$, so we choose values of K so as to explore the system near this value.

(a) Monte Carlo average $\langle O_X \rangle$ vs. J/h. **(b)** Monte Carlo average $\langle O_{Z_0 Z_1} \rangle$ vs. J/h.

Figure 3.11: Comparing analytical results obtained by exactly diagonalizing the quantum Hamiltonian $(1d)$ with the numerical results obtained from performing Monte Carlo on the effective classical model $(1 + 1d)$.

As can be seen from Fig. 3.11, the Monte Carlo averages of the corresponding classical observables matches with the thermal expectation values of the quantum operators. At higher values of J/h, we can see some deviations arising due to the *trotter error* despite the high MC acceptance rate.

Therefore, the modified Monte Carlo algorithm successfully on the two site problem, and we will verify its relevance for higher spatial lattice sizes N_x in the following section.

3.8 Comparing Monte Carlo against exact diagonalization

Analytical calculations for expectation values of quantum operators can only get us so far. The complexity of the calculation grows immensely on going from two sites to three sites. Therefore, it is not practical to rely on analytical calculations for evaluating quantum expectation values at higher lattice sizes $N_x > 2$. Instead, we use the machinery of numerical exact diagonalization (ED) to numerically diagonalize the Hamiltonian for expectation value calculations. The quantum expectation value (at finite temperature) of an observable $\hat{\mathcal{O}}$ is calculated as follows,

$$\langle \hat{\mathcal{O}} \rangle = \frac{1}{Z} \text{Tr}\left(e^{-\beta \hat{H}} \hat{\mathcal{O}}\right) = \frac{\sum_i \langle E_i | \hat{\mathcal{O}} | E_i \rangle \, e^{-\beta E_i}}{\sum_i \langle E_i | E_i \rangle \, e^{-\beta E_i}} \tag{3.8.1}$$

where we calculate the trace over the energy eigenbasis. These quantum thermal expecatation values can then be compared with the Monte Carlo averages of the corresponding classical observables.

For verification purposes, we take the highest spatial lattice size possible for exact diagonalization calculations, i.e., $N_x = 13$ (due to exponentially increasing computational and memory costs). This is also an interesting lattice size to work with since standard Metropolis Monte Carlo breaks the subsystem symmetries at this lattice size leading to biased sampling. The introduction of alignment flips restores ergodicity in our classical model, and this benchmarking will serve as a test to whether our modified Monte Carlo algorithm captures the correct dynamics of the quantum system.

3.8.1 Ground state simulations

The ground state properties of the quantum system are probed by considering the $\beta h \to \infty$ limit. This is because it is the combination βh (or βJ) which enters the partition function,

$$\exp\left[-\beta \hat{H}\right] = \exp\left[\beta h \left(\sum_i Z_i Z_{i+1} + \frac{J}{h} \sum_i X_i\right)\right]. \tag{3.8.2}$$

Thus, for the purposes of our ground state simulations, we choose $\beta h = 2.50$ ($\beta = 50$, $h = 0.05$). If we desire to simulate our model in the parameter range $J/h \in [a, b]$ and $\Delta \tau = 1$, then the range of K chosen for MC simulations is such that

$$K_i = -\frac{1}{2} \ln \tanh(h \cdot b), \qquad K_f = -\frac{1}{2} \ln \tanh(h \cdot a) \tag{3.8.3}$$
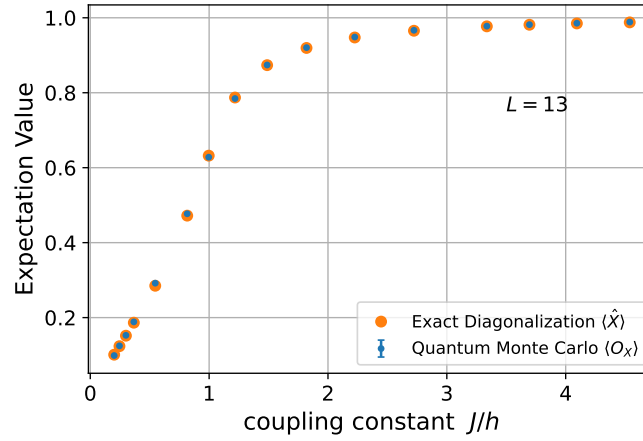
Monte Carlo setup

spatial lattice size $N_x = 13$

temporal lattice size $N_\tau = 50$

trotter unit $\Delta\tau = 1$

coupling parameter $Y = 0.05$

coupling parameter $K \in [0.76, 2.64]$

no of equilibration sweeps = 1.0e3

no of sampling sweeps $N_{\text{samp}} = 2\tau \cdot 1.0e4$

sampling step size = 2τ

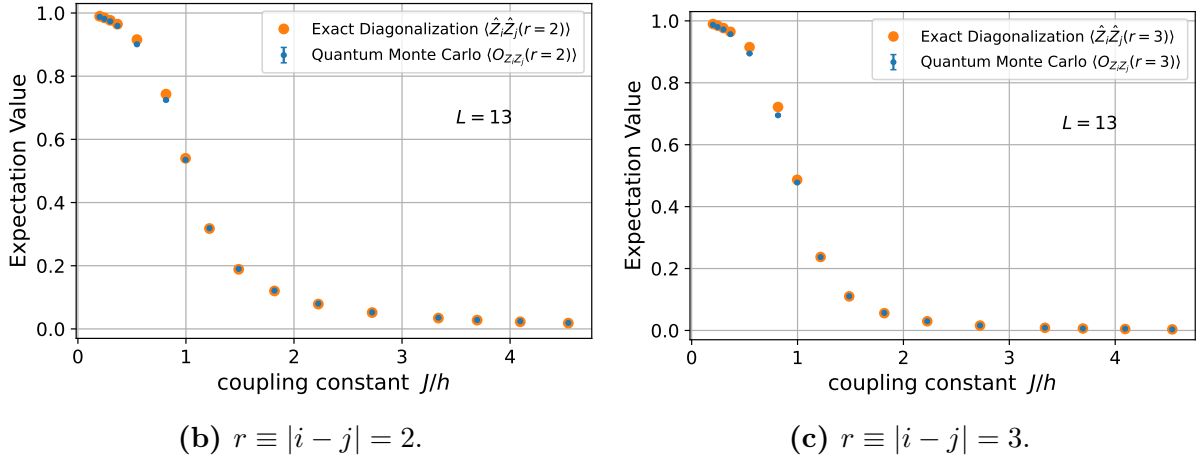**Exact diagonalization setup**

spatial lattice size $N_x = 13$

interaction parameter $h = 0.05$

field strength parameter $J \in [0.005, 0.22]$

inverse temperature $\beta = 50$

Figure 3.12: Comparing ED results for $\langle \hat{X} \rangle$ with MC average $\langle O_X \rangle$ at $\beta = 2.5$.

(a) $r \equiv |i - j| = 1$.

(b) $r \equiv |i - j| = 2$. **(c)** $r \equiv |i - j| = 3$.
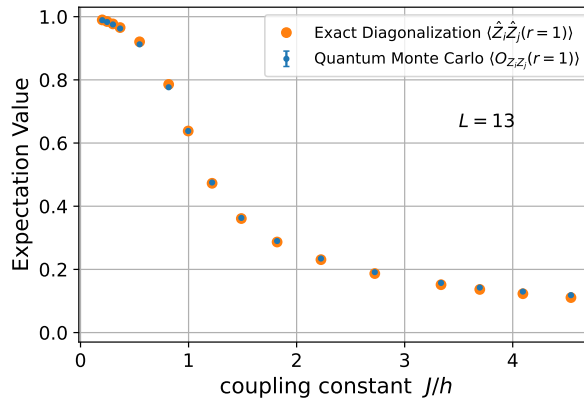
Figure 3.13: Comparing ED results for $\langle \hat{Z}_i \hat{Z}_j \rangle$ with MC average $\langle O_{Z_i Z_j} \rangle$ at $\beta = 2.5$.

The benchmark plots in Figs. 3.12 and 3.13 clearly show that the Monte Carlo averages match very closely (within error bars) with the exact diagonalization expectation values, except for the slight variations in $Z_i Z_j$ expectation values as $|i-j|$ increases, which appear due to periodic boundary effects.

3.8.2 Finite temperature simulations

The machinery of our quantum Monte Carlo simulations can also be used to perform finite temperature simulations of our model. Since $\beta h = Y \cdot N_\tau$ acts like a temperature scale in our model, we can simulate finite temperature features by choosing $\beta h < 1$.

Monte Carlo setup

Ideally, for a Monte Carlo simulation, having a large value of N_τ is necessary for reducing the trotter error and ensuring convergence to the correct results. Therefore, for the $Y \cdot N_\tau < 1$ combination, Y should be as small as possible while also ensuring that the order of magnitude stays roughly the same as K (to prevent freezing of spins along the spatial axis).

The only relevant parameters entering the Monte Carlo calculation are Y, K, and N_τ. We choose $Y = 0.05$, the same as before, and $N_\tau = 10$, implying that the value of the temperature scale is $\beta h = Y \cdot N_\tau = 0.5$. The values of K are chosen accordingly to explore the region close to $J/h = 1$.

The parameters are chosen as follows

    spatial lattice size $N_x = $ 13

    temporal lattice size $N_\tau = $ 10

    trotter unit $\Delta\tau = 1$

    coupling parameter $Y = 0.05$

```
coupling parameter K ∈ [1.15, 2.30]

no of equilibration sweeps = 1.0e3

no of sampling sweeps N_samp = 2τ · 1.0e4

sampling step size = 2τ
```

Exact diagonalization setup

The exact diagonalization calculations doesn't suffer from a spin freezing or trotterization error problem like the Monte Carlo simulations. Moreover, the expectation value calculation for a fixed value of J/h only depends on the value of βh. This implies that we have a family of parameter pair solutions (β, h) which satisfy the constraint $\beta h = C$ where C is our desired temperature scale for the simulation. This family of parameter pairs $(\beta, h = C/\beta)$ gives the same results for the expectation value calculations.

Thus, exploiting this extra degree of freedom, we pretend to work at unit temperature $\beta = 1$ in exact diagonalization calculations. Consequently, h and J are chosen as follows

$$h = \beta h = N_\tau Y \tag{3.8.4a}$$

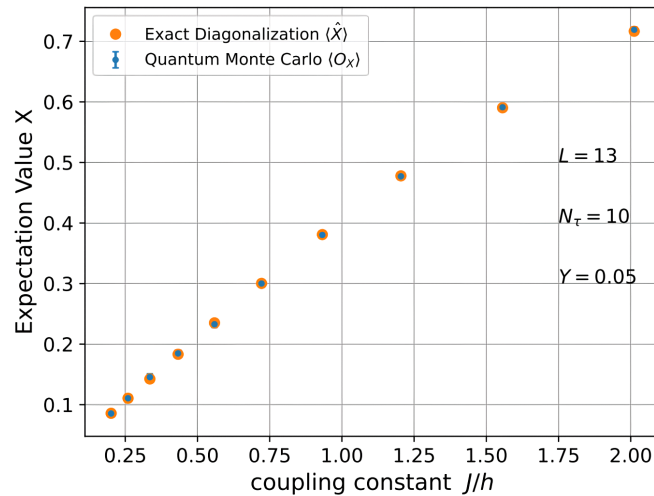$$J = \beta J = N_\tau \operatorname{arctanh}(e^{-2K}) \tag{3.8.4b}$$

where Y value and K ranges are chosen to be the same as the Monte Carlo parameters. The parameters are chosen as follows
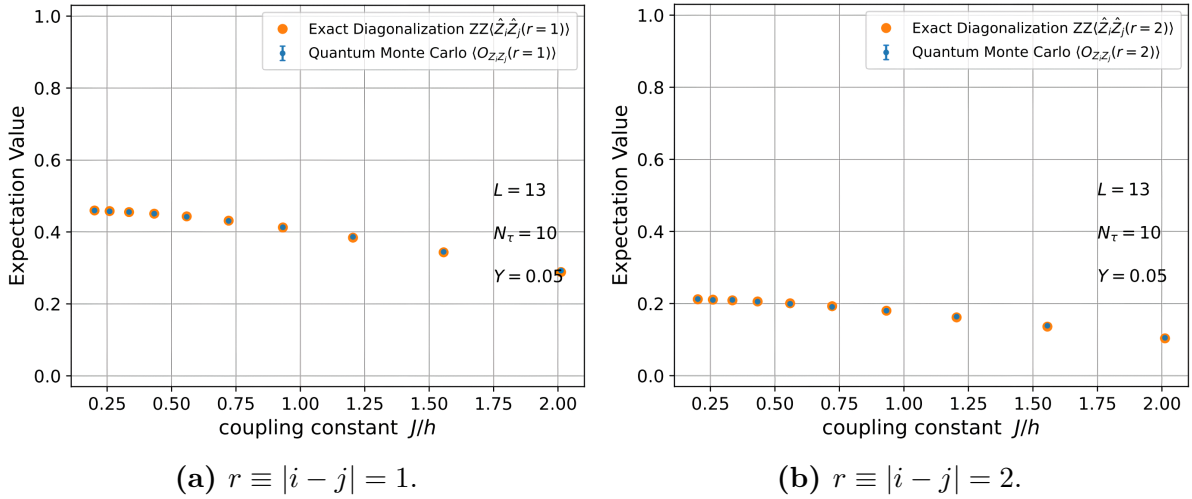
```
spatial lattice size N_x = 13

interaction parameter h = N_τ Y = 0.05

field strength parameter J = N_τ arctanh(e^{-2K}) ∈ [0.01, 0.1]

inverse temperature β = 1
```


Figure 3.14: Comparing ED results for $\langle \hat{X} \rangle$ with MC average $\langle O_X \rangle$ at $\beta = 0.5$.

(a) $r \equiv |i - j| = 1$. **(b)** $r \equiv |i - j| = 2$.

Figure 3.15: Comparing ED results for $\langle \hat{Z}_i \hat{Z}_j \rangle$ with MC average $\langle O_{Z_i Z_j} \rangle$ at $\beta = 0.5$.

Figs. 3.14 and 3.15 again show very close matching of Monte Carlo averages with the exact diagonalization calculations, even at finite temperatures $\beta h < 1$.

Thus, the ergodicity analysis and the benchmarking against exact digaonlization clearly suggest that our modified Metropolis Monte Carlo simulations are successful in simulating the model of interest. Therefore, we conclude that the proposed Metropolis algorithm is an effective numerical tool for understanding the phase structure of $\mathbb{Z}_2$ lattice gauge theory.

3.9 Quantum phase transition

The study of expectation values of operators in the previous sections highlighted variation in the value of the quantities at $T = 0$ as the coupling parameter J/h is varied across a range. The variation of these quantities from a zero to a non-zero value is illustrates a change in phase. Since such a phase transition isn't driven by any thermal effects and is purely an artefact of the quantum fluctuations tuned by a variation in the nonthermal parameters, it is called a *quantum phase transition*.

Bibliography

[1] Somendra M Bhattacharjee and Flavio Seno. "A measure of data collapse for scaling". In: *Journal of Physics A: Mathematical and General* 34.33 (Aug. 2001), pp. 6375–6380. DOI: 10.1088/0305-4470/34/33/302. URL: https://doi.org/10.1088%2F0305-4470%2F34%2F33%2F302.

[2] Umberto Borla et al. "Quantum phases of two-dimensional $\mathbb{Z}_2$ gauge theory coupled to single-component fermion matter". In: *Phys. Rev. B* 105 (7 Feb. 2022), p. 075132. DOI: 10.1103/PhysRevB.105.075132. URL: https://link.aps.org/doi/10.1103/PhysRevB.105.075132.

[3] P H Y Li, R F Bishop, and C E Campbell. "A frustrated spin-1 $J_1 - J_2$ Heisenberg antiferromagnet: An anisotropic planar pyrochlore model". In: *Journal of Physics: Conference Series* 529.1 (Aug. 2014), p. 012008. DOI: 10.1088/1742-6596/529/1/012008. URL: https://dx.doi.org/10.1088/1742-6596/529/1/012008.

[4] Manu Mathur and T. P. Sreeraj. "Lattice gauge theories and spin models". In: *Phys. Rev. D* 94 (8 Oct. 2016), p. 085029. DOI: 10.1103/PhysRevD.94.085029. URL: https://link.aps.org/doi/10.1103/PhysRevD.94.085029.

[5] Yong-Zhi Ren, Ning-Hua Tong, and Xin-Cheng Xie. "Cluster mean-field theory study of J1-J2 Heisenberg model on a square lattice". In: *Journal of Physics: Condensed Matter* 26.11 (Mar. 2014), p. 115601. DOI: 10.1088/0953-8984/26/11/115601. URL: https://dx.doi.org/10.1088/0953-8984/26/11/115601.

[6] Masuo Suzuki. "Relationship between d-Dimensional Quantal Spin Systems and (d+1)-Dimensional Ising Systems: Equivalence, Critical Exponents and Systematic Approximants of the Partition Function and Spin Correlations". In: *Progress of Theoretical Physics* 56.5 (Nov. 1976), pp. 1454–1469. ISSN: 0033-068X. DOI: 10.1143/PTP.56.1454. eprint: https://academic.oup.com/ptp/article-pdf/56/5/1454/5264429/56-5-1454.pdf. URL: https://doi.org/10.1143/PTP.56.1454.

[7] Franz J. Wegner. *Duality in generalized Ising models*. 2014. arXiv: 1411.5815 [hep-lat].